



Genetic ablation of pannexin1 counteracts liver fibrosis in a chemical, but not in a surgical mouse model

Sara Crespo Yanguas¹ · Tereza C. da Silva² · Isabel V. A. Pereira² · Michaël Maes¹ · Joost Willebrords¹ · Valery I. Shestopalov^{3,4} · Bruna M. Goes² · Marina Sayuri Nogueira⁵ · Inar Alves de Castro⁵ · Guilherme R. Romualdo⁶ · Luís F. Barbisan⁶ · Eva Gijbels¹ · Mathieu Vinken¹ · Bruno Cogliati²

Received: 17 October 2017 / Accepted: 3 July 2018 / Published online: 9 July 2018
© Springer-Verlag GmbH Germany, part of Springer Nature 2018

Abstract

Liver fibrosis is the final common pathway for almost all causes of chronic liver injury. This chronic disease is characterized by excessive deposition of extracellular matrix components mainly due to transdifferentiation of quiescent hepatic stellate cell into myofibroblasts-like cells, which in turn is driven by cell death and inflammation. In the last few years, paracrine signaling through pannexin1 channels has emerged as a key player in the latter processes. The current study was set up to investigate the role of pannexin1 signaling in liver fibrosis. Wild-type and whole body pannexin1 knock-out mice were treated with carbon tetrachloride or subjected to bile duct ligation. Evaluation of the effects of pannexin1 deletion was based on a number of clinically relevant read-outs, including markers of liver damage, histopathological analysis, oxidative stress, inflammation and regenerative capacity. In parallel, to elucidate the molecular pathways affected by pannexin1 deletion as well as to mechanistically anchor the clinical observations, whole transcriptome analysis of liver tissue was performed. While pannexin1 knock-out mice treated with carbon tetrachloride displayed reduced collagen content, hepatic stellate cell activation, inflammation and hepatic regeneration, bile duct ligated counterparts showed increased hepatocellular injury and antioxidant enzyme activity with a predominant immune response. Gene expression profiling revealed a downregulation of fibrotic and immune responses in pannexin1 knock-out mice treated with carbon tetrachloride, whereas bile duct ligated pannexin1-deficient animals showed a pronounced inflammatory profile. This study shows for the first time an etiology-dependent role for pannexin1 signaling in experimental liver fibrosis.

Keywords Pannexin1 · Liver fibrosis · Inflammation · Stellate cells

Abbreviations

α -SMA	Alpha smooth muscle actin
ALT	Alanine aminotransferase
ALP	Alkaline phosphatase
ANOVA	Analysis of variance

Mathieu Vinken and Bruno Cogliati share equal seniorship.

Electronic supplementary material The online version of this article (<https://doi.org/10.1007/s00204-018-2255-3>) contains supplementary material, which is available to authorized users.

✉ Bruno Cogliati
bcogliati@usp.br

- ¹ Department of In Vitro Toxicology and Dermato-Cosmetology, Vrije Universiteit Brussel, Brussels, Belgium
- ² Department of Pathology, School of Veterinary Medicine and Animal Science, University of São Paulo, São Paulo, Brazil
- ³ Bascom Palmer Eye Institute, Department of Ophthalmology, University of Miami Miller School of Medicine, Miami, USA

- ⁴ Department of Cell Biology and Anatomy, University of Miami Miller School of Medicine, Miami, USA
- ⁵ Department of Food and Experimental Nutrition, Faculty of Pharmaceutical Sciences, University of São Paulo, São Paulo, Brazil
- ⁶ Department of Pathology, Botucatu Medical School, UNESP-São Paulo State University, Botucatu, SP, Brazil

ASC	Apoptosis-associated speck-like protein containing a C-terminal caspase-recruitment domain
AST	Aspartate aminotransferase
ATP	Adenosine-5'-triphosphate
BDL	Bile duct ligation
Casp1	Caspase 1
CCl ₄	Carbon tetrachloride
Clec7a	Dectin-1
Colla1	Collagen type 1 alpha 1
Cxcl14	Chemokine ligand 14
GPx	Glutathione peroxidase
GR	Glutathione reductase
HSCs	Hepatic stellate cells
IL	Interleukin
ip	Intraperitoneally
Lbp	Lipopolysaccharide-binding protein
Loxl2	Lysyl oxidase-like 2
Ly96	Lymphocyte antigen 96
MCP-1	Monocyte chemoattractant protein 1
MIP1 γ	Macrophage protein 1 gamma
Nalp3	NACHT, LRR, and pyrin domain-containing protein 3
<i>n</i>	Number or repeats
NF- κ B	Nuclear factor kappa B
Panx	Pannexin
<i>p</i>	Probability
RT-qPCR	Reverse transcription quantitative real-time polymerase chain reaction
S100a9	S100 calcium-binding protein A9
SEM	Standard error of mean
SOD	Superoxide dismutase
sTNF-RI/-RII	Soluble TNF receptor 1/2
TCA-3	T-cell activation protein 3
TECK	Thymus-expressed chemokine
TLR	Toll-like receptor
TNF α	Tumor necrosis factor alpha
WT	Wild-type

attention. Immune cells participate in the promotion of hepatocellular damage, the activation and survival of HSCs and fibrosis regression (Seki and Schwabe 2015). Indeed, blockage of macrophage infiltration inhibits HSC activation and attenuates fibrotic responses (Imamura et al. 2005; Pradere et al. 2013). The mechanisms driving cellular attraction mainly involve paracrine communication circuits, including adenosine-5'-triphosphate (ATP) signaling. Upon injury, apoptotic cells release ATP and uridine-5'-triphosphate into the extracellular milieu via pannexin1 (Panx1), which act as “find-me” signals to attract monocytes, macrophages and microglia to the area of the insult (Chekeni et al. 2010; Davalos et al. 2005). In addition, extracellular ATP potentiates HSC activation in a NACHT, LRR, and pyrin domain-containing protein 3 (Nalp3) inflammasome-dependent manner, in turn contributing to the generation of the pro-inflammatory cytokines interleukin 1 beta, 6 and 18 (IL1 β /6/18) (Jiang et al. 2017). Panx channels have been recently identified as critical mediators in ATP release (Dahl 2015). The Panx family consists of 3 members, called Panx1-3, with the former being the most widespread isoform. In the liver, Panx1 was reported to be expressed by hepatocytes, Kupffer cells and HSCs (Kim et al. 2015; Willebrords et al. 2017b; Xiao et al. 2012). In addition to playing a role in physiological conditions, Panx1 channels underlie cell death and inflammatory processes. The latter involves the activation of the Nalp3 inflammasome complex and initiation of leukocyte migration (Crespo Yanguas et al. 2017). In fact, in cardiac fibrosis, cardiomyocytes release ATP through Panx1 channels leading to early fibroblast activation and subsequent expression of IL1 β (Dolmatova et al. 2012). This supports the notion that extracellular ATP participates in myofibroblast activation pathways, which in turn trigger immune-related responses. In this study, it is tested whether a similar scenario takes place in liver fibrosis. For this purpose, liver fibrosis was experimentally induced through administration of carbon tetrachloride (CCl₄) or application of bile duct ligation (BDL) to both wild-type (WT) and Panx1^{-/-} mice.

Introduction

Liver fibrosis is a wound healing response to chronic injury characterized by excessive extracellular matrix deposition. At the cellular level, the main contributors to the fibrotic response are activated hepatic stellate cells (HSCs) (Puche et al. 2013). This activation program is a complex cellular signaling process in which HSCs interact with hepatocytes, sinusoidal endothelial cells, Kupffer cells and infiltrating immune cells (Canbay et al. 2003; Karlmark et al. 2009; Pradere et al. 2013; Xie et al. 2012). In the past decade, the role of the immune response in both progression and regression of chronic liver diseases has gained increasing

Materials and methods

Animals and treatment

Male WT C57BL/6 mice were obtained from Jackson Laboratories (USA). The generation of the global Panx1^{-/-} mice (CMV-Cre/Panx1) was previously described (Dvoriantchikova et al. 2012). Animals were housed in the animal facility of the School of Veterinary Medicine and Animal Science of the University of São Paulo-Brazil. Mice were kept in a room with ventilation (i.e., 16–18 air changes/hour), relative humidity (i.e., 45–65%), controlled temperature (i.e.,

20–24 °C) and light/dark cycle 12:12 and were given water and balanced diet (NUVILAB-CR1, Nuvital Nutrientes LTDA, Brazil) ad libitum. This study has been approved by the Committee on Bioethics of the School of Veterinary Medicine and Animal Science of the University of São Paulo-Brazil (protocol number 9999100314) and all animals received humane care according to the criteria outlined in the “Guide for the Care and Use of Laboratory Animals”.

Eight-week old mice of each genotype were used and received 3 intraperitoneal (ip) injections of 20% v/v CCl₄ (Sigma-Aldrich, Brazil) per week diluted in corn oil for 8 weeks. Specifically, 1 µl CCl₄ per g body weight was administered for the first 2 weeks. Thereafter, a weekly increment of 0.25 µl CCl₄ per g body weight to the utmost dose of 2 µl CCl₄ per g body weight was given to the animals. Corresponding controls for both genotypes relied on the administration of corn oil ip (Oil). In parallel, a BDL mouse model was set up as described elsewhere (Tag et al. 2015). For this purpose, 8- to 12-weeks old mice from each genotype were used. All mice were weighed and sacrificed after 8 weeks of CCl₄ treatment or 20 days after BDL by exsanguination during sampling under isoflurane-induced anesthesia. Blood collected by cardiac puncture was drawn into a heparinized syringe and centrifuged for 10 min at 1503×g, and serum was stored at – 20 °C. Livers were excised and fragments were fixed in 10% phosphate-buffered formalin or snap-frozen in liquid nitrogen with storage at – 80 °C.

Histopathological liver examination and collagen analysis

For microscopic evaluation, formalin-fixed liver fragments were embedded in paraffin and 5 µm sections were stained with hematoxylin-eosin (H&E) or Sirius red for blinded evaluation of the liver as previously described (Cogliati et al. 2011). Morphometric analysis of Sirius red staining was performed in 10 randomly selected fields per section from the left lobe (10× objective) using a Nikon Eclipse Ti microscope (Nikon, Japan). Semi-quantitative analysis of the fibrosis area was performed with ImageJ (National Institutes of Health, Bethesda, MD) (Schindelin et al. 2015) and calculated by the formula [area of fibrosis (%) = total fibrosis area/total area of the liver tissue].

Analysis of serum biochemical parameters

Serum levels of alanine aminotransferase (ALT; IU/L), aspartate aminotransferase (AST; IU/L), alkaline phosphatase (ALP; IU/L), conjugated and total bilirubin (mg/dL) and albumin (g/dL) were measured with an automated spectrophotometric Labmax 240 analyzer (Labtest Diagnostica, Brazil) after appropriate dilution of samples.

Immunohistochemistry

Immunoreactivity for α-smooth muscle actin (α-SMA), CD68 or Ki-67 was performed as described elsewhere (Cogliati et al. 2011) with slight modifications. Briefly, 5-µm liver sections were subjected to antigen retrieval at 120 °C for 5 min in a Pascal Pressure Chamber (Dako Cytomation, Denmark) and blocked during 15 min. Then, slides were treated with low-fat milk for 60 min and incubated in a humidified chamber overnight at 4 °C with the appropriate antibodies (Abcam, UK). Subsequently, slides were incubated with a one-step polymer-HRP (EasyPath—Erviegas, Brazil) for 20 min, developed with 3×3-diaminobenzidine chromogen (Sigma-Aldrich, USA) and counterstained with Harris hematoxylin. Semi-quantitative analysis was performed using Image-Pro Plus 4.5 software (Media Cybernetics, USA) in 10 randomly selected fields (20× objective for α-SMA and 40× objective for CD68 and Ki-67) per section from the left lobe. Data analysis was based on the following calculations [α-SMA area (%) = α-SMA⁺ area/(total field area – vascular luminal area)], [CD68⁺ density = CD68⁺ cells/total field area (mm²)] and [Ki-67⁺ density = Ki-67⁺ cells/total field area (mm²)].

Immunofluorescence

The cellular distribution of T-lymphocytes, monocytes, granulocytes and neutrophils was determined by immunofluorescence as previously described (Maes et al. 2016), with slight modifications. Briefly, 10 µm liver sections from flash-frozen liver tissue were fixated with acetone (CD3, Ly6c and Ly6g) or methanol (CD11b) for 10 min at – 20 °C. Liver sections were incubated with primary antibodies directed against CD3 (Abcam, UK), CD11b (Abcam, UK), Ly6c (Abcam, UK) and Ly6g (Abcam, UK) diluted in blocking buffer based on 5% w/v donkey serum (Jackson ImmunoResearch Inc., USA) and 1% w/v bovine serum albumin (Sigma-Aldrich, USA) dissolved in phosphate-buffered saline for 1 h at 37 °C. After intensive washing, liver sections were incubated for 1 h at room temperature against polyclonal donkey anti-rabbit Alexa Fluor[®] 488-conjugated secondary antibody (Jackson ImmunoResearch Inc., USA) or polyclonal goat anti-rat Alexa Fluor[®] 488-conjugated secondary antibody (Abcam, UK) diluted in blocking buffer. Thereafter, Vectashield with DAPI (Vector laboratories, USA) was used to stain the nuclei and as a mounting medium. Detection was performed by fluorescence microscope Nikon Eclipse Ti (Nikon, Japan).

Analysis of hepatic antioxidant enzymes

The activity of superoxide dismutase (SOD), glutathione peroxidase (GPx), glutathione reductase (GR) and catalase was assayed as previously described (Cogliati et al. 2016). Enzymatic activity was expressed in U/mg protein.

Immunoblot analysis

Immunoblot analysis of liver tissue was performed as previously described (Maes et al. 2017) with slight modifications. After electrophoresis and blotting, blocking of the nitrocellulose membranes was performed with 5% w/v bovine serum albumin (Sigma-Aldrich, USA) in Tris-buffered saline solution containing 0.1% Tween 20. Membranes were incubated overnight at 4 °C with primary antibody directed against p-NF- κ Bp65 S536 (Cell signaling, USA) and β -actin (Abcam, UK) followed by incubation for 1 h at room temperature with appropriate secondary antibody. Detection of the proteins was carried out by means of an enhanced chemiluminescence. For semi-quantification purposes, a recently described normalization method based on the total protein loading was used to overcome the drawbacks exerted by the use of housekeeping proteins (Eaton et al. 2013; Rivero-Gutiérrez et al. 2014; Taylor et al. 2013; Taylor and Posch 2014), including (1) the lack of expression in a uniform manner within the experimental

conditions (Eaton et al. 2013; Rivero-Gutiérrez et al. 2014). (2) The protein working range in which the linearity is maintained may differ between the housekeeping and the protein of interest (Chen and Xu 2015; Eaton et al. 2013; Taylor et al. 2013). (3) Data normalization with housekeeping proteins relies on a single data point, providing a poor reflection of inconsistencies. Consequently, p-NF- κ Bp65 S536 signals were normalized against total protein loading and expressed as relative alterations compared to BDL-subjected or CCl₄-treated WT mice.

Analysis of liver inflammatory markers

Inflammatory markers were determined in hepatic homogenates using a mouse inflammation antibody array (Abcam, UK) following manufacturer's instructions. Briefly, antibody-bound membranes were blocked during 30 min at room temperature. Thereafter, blocked membranes were exposed to 250 μ g protein/ml blocking buffer overnight at 4 °C while shaking. Membranes were washed, incubated with biotin-conjugated anti-cytokines for 2 h at room temperature, washed and exposed to horseradish peroxidase-conjugated streptavidin for 2 h at room temperature. Following washing, proteins were detected by means of enhanced chemiluminescence and visualized by Chemidoc™ MP system (Bio-Rad, USA).

Table 1 The Taqman probes and primers used for RT-qPCR analysis

Gene	Assay ID	Accession number	Assay location	Amplicon size (base pairs)	Exon boundary
<i>Actb</i>	Mm00607939_s1	NM_007393.3	1233	115	6–6
<i>ASC</i>	Mm00445747_g1	NM_023258.4	487	73	1–2
<i>B2m</i>	Mm00437762_m1	NM_009735.3	111	77	1–2
<i>Casp1</i>	Mm00438023_m1	NM_009807.2	532	99	3–4
<i>Clec7a</i>	Mm01183349_m1	NM_020008.2	294	77	2–3
<i>Coll1a1</i>	Mm00801666_g1	NM_007742.3	4071	89	49–50
<i>Cxcl14</i>	Mm00444699_m1	NM_019568.2	660	64	3–4
<i>Gapdh</i>	Mm99999915_g1	NM_008084.2	265	107	2–3
<i>Hmbs</i>	Mm01143545_m1	NM_013551.2	473	81	6–7
<i>Lbp</i>	Mm00493139_m1	NM_008489.2	1578	90	14–15
<i>Loxl2</i>	Mm00804740_m1	NM_033325.2	2390	82	13–14
<i>Ly96</i>	Mm01227593_m1	NM_001159711.1	329	119	3–4
<i>Nalp3</i>	Mm00840904_m1	NM_145827.3	499	84	2–3
<i>Panx1</i>	Mm00450900_m1	NM_019482.2	986	70	3–4
<i>S100a9</i>	Mm00656925_m1	NM_001281852.1	212	162	2–3
<i>Ubc</i>	Mm02525934_g1	NM_019639.4	370	176	2–2

Assay identification (ID) and accession number of target and reference genes are indicated

Actb β -actin, *ASC* apoptosis-associated speck-like protein containing a C-terminal caspase-recruitment domain, *B2m* β -2-microglobulin, *Casp1* caspase 1, *Clec7a* dectin-1, *Coll1a1* collagen type 1 alpha 1, *Cxcl14* chemokine ligand 14, *Gapdh* glyceraldehyde 3-phosphate dehydrogenase, *Hmbs* hydroxymethylbilane synthase, *Lbp* lipopolysaccharide-binding protein, *Loxl2* lysyl oxidase-like 2, *Ly96* lymphocyte antigen 96, *Panx1* pannexin1, *S100a9* S100 calcium-binding protein A9, *Nalp3* NACHT, LRR, and pyrin domain-containing protein 3, *Ubc* ubiquitin C)

Semi-quantitative results were obtained after densitometric analysis. Thereafter, background was subtracted from each data point and results were normalized against the positive controls provided by biotin-conjugated IgG. Final

results were presented as relative signal intensity against sham-subjected or oil-treated WT mice.

Fig. 1 Panx1 RNA expression in liver fibrosis. WT mice ($n = 10–15$) were treated with 20% CCl₄ or Oil for 8 weeks and subjected to BDL or sham for 20 days. Results were analyzed by *t* test with Welch's correction. Data were expressed as means \pm SEM (** $p \leq 0.001$; **** $p \leq 0.0001$)

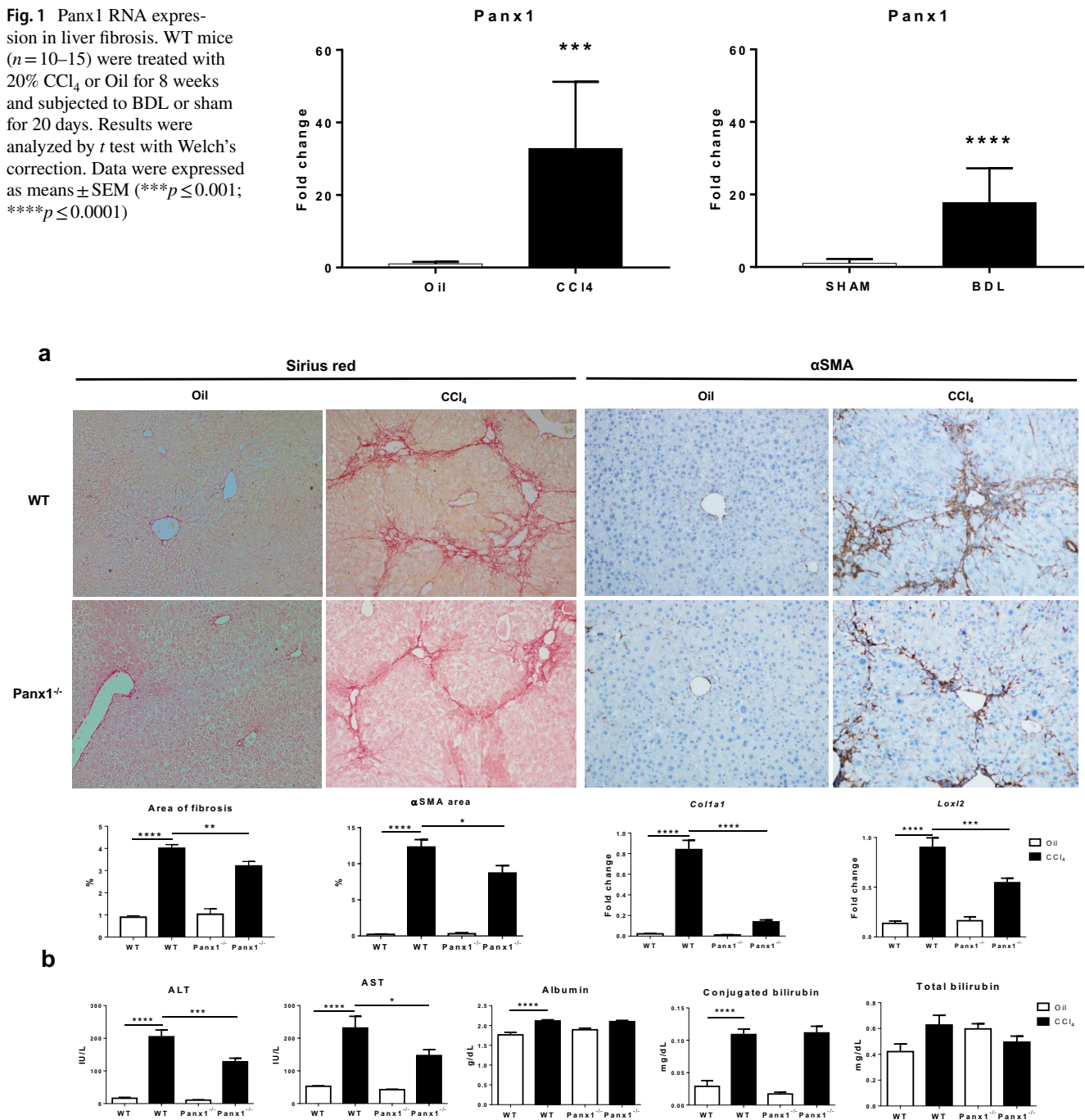


Fig. 2 Effect of genetic Panx1 deficiency on hepatocellular injury and liver fibrogenesis in chemically-induced liver fibrosis. WT and Panx1^{-/-} mice ($n = 5–15$) were administered 20% CCl₄ ip at a gradually increased dose for 8 weeks. **a** Area of fibrosis, area of α -SMA-positive cells, and *Col1a1* and *Lox12* RNA levels were evaluated. **b**

Serum levels of ALT, AST, albumin, total and conjugated bilirubin were determined. Results were analyzed by one-way ANOVA followed by post hoc tests using Bonferroni correction. Data were expressed as means \pm SEM (* $p \leq 0.05$; ** $p \leq 0.01$; *** $p \leq 0.001$; **** $p \leq 0.0001$)

Reverse transcription quantitative real-time polymerase chain reaction analysis

Reverse transcription quantitative real-time polymerase chain reaction (RT-qPCR) analysis of liver tissue was assayed as explained elsewhere (Maes et al. 2017). The Taqman probes and primers specific for the target and reference genes are represented in Table 1. Relative alterations (fold change) in RNA levels were calculated according to the $2^{(-\Delta\Delta Cq)}$ formula (Livak and Schmittgen 2001).

Whole transcriptome analysis

Transcriptomic analysis was performed as previously described (Willebrords et al. 2017a, b) with slight modifications. After RNA extraction, integrity was assessed by microfluidic analysis using a Fragment Analyzer (Avanced

Analytical Technologies, USA). A total of 100 ng RNA per sample was amplified with a Genechip 3' IVT Express Kit, thereby following the manufacturer's instructions (Affymetrix, Germany) and purified with magnetic beads. Subsequently, 12.5 μ g fragmented amplified RNA was hybridized to Affymetrix Clariom™ D mouse arrays and placed in a Genechip Hybridization Oven-645 (Affymetrix, Germany) rotating at 60 rpm at 45 °C for 16 h. Thereafter, the arrays were washed and stained. The chips were scanned and quality control matrices were confirmed following the manufacturer's guidelines. Background correction, summarization and normalization of all data were done with Expression Console and Affymetrix Transcriptome Analysis Console Software.

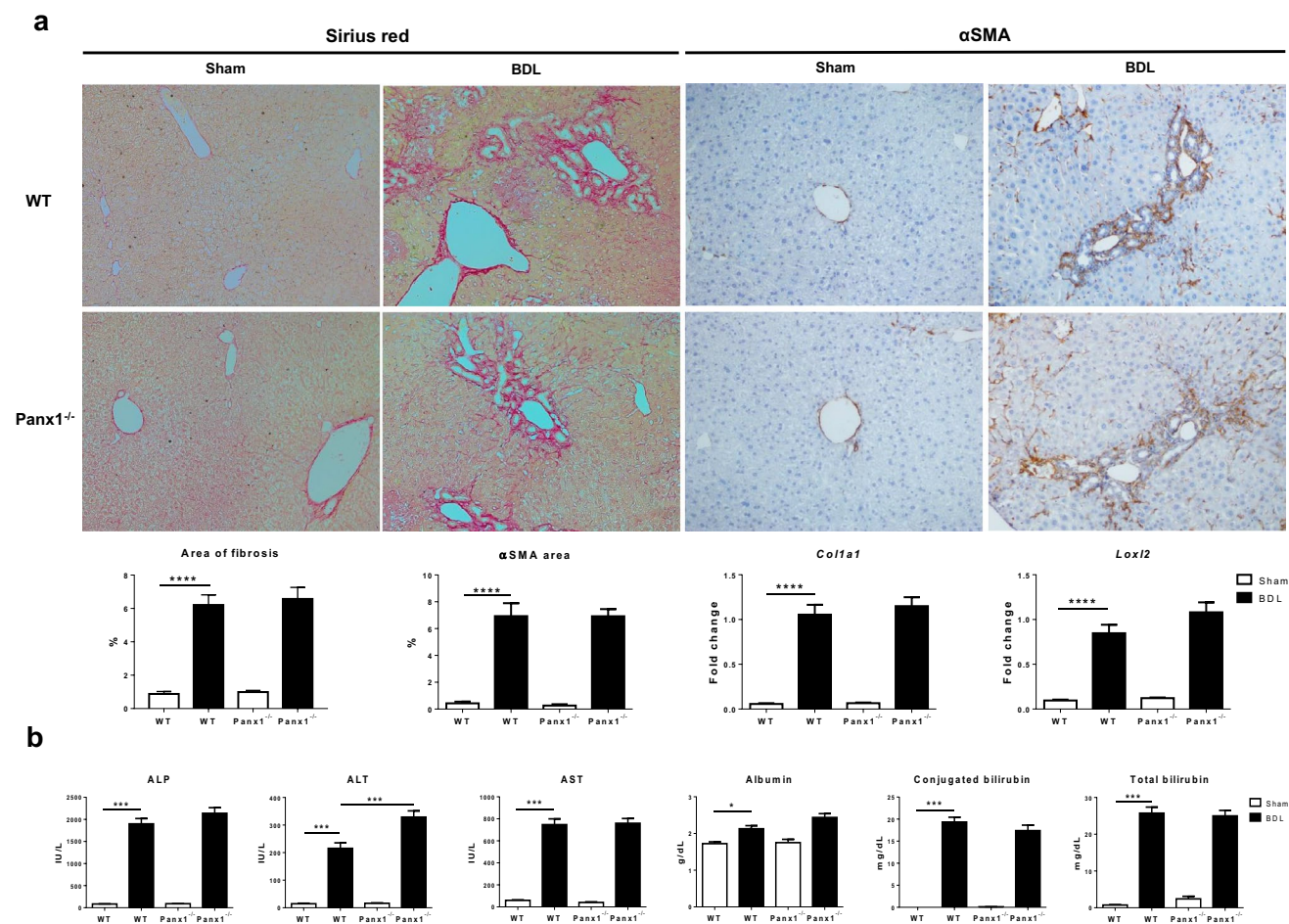


Fig. 3 Effect of genetic Panx1 deficiency on hepatocellular injury and liver fibrogenesis in surgically-induced liver fibrosis. WT and Panx1^{-/-} mice ($n=5-15$) were subjected to BDL for 20 days. **a** Area of fibrosis, area of α -SMA-positive cells, and *Col1a1* and *Loxl2* RNA levels were evaluated. **b** Serum levels of ALP, ALT, AST, albumin,

total and conjugated bilirubin were determined. Results were analyzed by one-way ANOVA followed by post hoc tests using Bonferroni correction. Data were expressed as means \pm SEM ($*p \leq 0.05$; $***p \leq 0.001$; $****p \leq 0.0001$)

Statistical analysis

The number of repeats (n) for each type of analysis varied and is specified in the discussion of the results. All data were expressed as mean \pm standard error of the mean (SEM) or median \pm interquartile. Results were statistically processed by t tests with Welch's correction, one-way analysis of variance (ANOVA) followed by post hoc tests with Bonferroni correction or Kruskal–Wallis tests followed by post hoc tests using Dunn's correction depending on the distribution (D'Agostino–Pearson normality test for large n or Shapiro–Wilk normality test for low n) using GraphPad Prism7 software with probability (p) values of less than or equal to 0.05 considered as significant.

Results

Panx1 expression in liver fibrosis

A number of reports have described upregulated Panx1 expression levels as a consequence of liver disease (Csak et al. 2011; Kim et al. 2015; Maes et al. 2017). RT-qPCR analysis was used to assess Panx1 expression levels in experimental liver fibrosis in WT mice upon CCl₄ or BDL. Panx1 RNA expression levels were increased in both the CCl₄ mouse model ($p \leq 0.001$) and the BDL mouse model ($p \leq 0.0001$) in comparison with their untreated controls (Fig. 1).

Effects of genetic Panx1 deficiency on hepatocellular injury and liver fibrogenesis

CCl₄-treated Panx1^{-/-} animals displayed less collagen accumulation ($p \leq 0.01$) as well as decreased amounts of α -SMA⁺ cells ($p \leq 0.05$) in comparison with WT counterparts. In addition, RT-qPCR analysis revealed down-regulated expression of collagen type 1 alpha 1 (*Coll1a1*) and lysyl oxidase-like 2 (*Loxl2*) ($p \leq 0.001$) (Fig. 2a). Furthermore, CCl₄-treated Panx1^{-/-} animals showed lowered serum ALT and AST levels ($p \leq 0.001$), but no changes in albumin and total and conjugated bilirubin (Fig. 2b).

In the BDL group, no alterations in collagen accumulation or expression of HSC activation markers were noticed between Panx1^{-/-} and WT mice (Fig. 3a). Nevertheless, hepatic damage was exacerbated in BDL-subjected Panx1^{-/-} mice as evidenced by higher levels of serum ALT ($p \leq 0.001$), yet with unchanged quantities of ALP, AST, albumin, conjugated and total bilirubin (Fig. 3b).

Effect of genetic Panx1 deficiency on oxidative stress in liver fibrosis

Oxidative stress with generation of free radicals and lipid peroxidation constitutes an important hallmark in the pathophysiological mechanisms underlying fibrogenesis (Gandhi 2012). Accordingly, the activity of several oxidative stress scavengers was measured in liver tissue. CCl₄-treated Panx1^{-/-} mice showed an increase in SOD activity ($p \leq 0.01$) and no changes in GPx, GR and

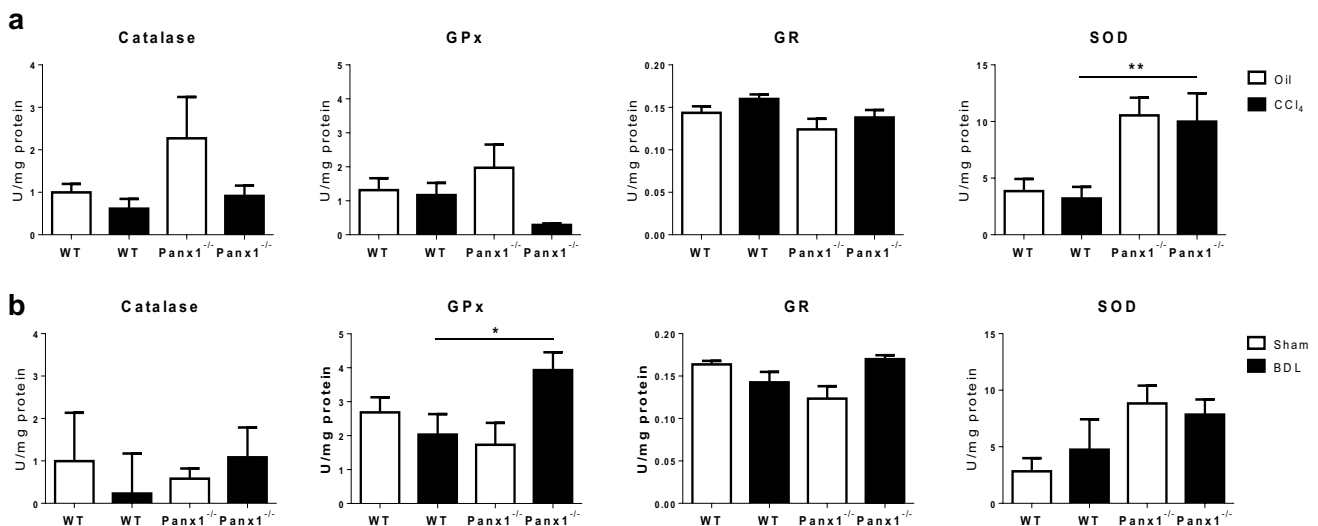


Fig. 4 Effect of genetic Panx1 deficiency on oxidative stress in liver fibrosis. WT and Panx1^{-/-} mice ($n=8$) were administered 20% CCl₄ ip at a gradually increased dose for 8 weeks or subjected to BDL for 20 days. Activity of catalase, GPx, GR and SOD was evaluated in **a** the CCl₄ model and **b** the BDL model. Results were analyzed by one-

way ANOVA followed by post hoc tests using Bonferroni correction and with Kruskal–Wallis test followed by post hoc tests using Dunn's correction in case of SOD in the CCl₄ model as well as catalase and SOD in the BDL model. Data were expressed as means \pm SEM or median \pm interquartile (* $p \leq 0.05$; ** $p \leq 0.01$)

catalase activities (Fig. 4a). $Panx1^{-/-}$ mice subjected to BDL displayed increased activity of GPx ($p \leq 0.05$) with SOD, GR and catalase being unmodified (Fig. 4b).

Effect of genetic $Panx1$ deficiency on inflammation in liver fibrosis

Hepatic macrophages participate in the regulation of the severity of the fibrotic response mainly by promotion of hepatocellular damage and the initiation and survival of activated HSCs (Cai et al. 2017; Seki and Schwabe 2015; Woolbright and Jaeschke 2012). A key mechanism driving the survival of activated HSCs is the activation of nuclear factor kappa B (NF- κ B) by tumor necrosis factor alpha (TNF α) and IL1 β (Pradere et al. 2013). In this study, the number of macrophages was monitored through staining and counting of CD68⁺ cells in liver tissue. CD68⁺ cells

were mainly located in the sinusoids of untreated animals, while in CCl₄-treated or BDL-subjected mice, these cells were predominantly found in areas surrounding the scar tissue. In the CCl₄ mouse model, the CD68⁺ cell population was not changed upon genetic $Panx1$ ablation (Fig. 5a). Furthermore, evaluation of NF- κ B activation through semi-quantitative immunoblot analysis showed reduced protein levels of NF- κ B p65 phosphorylated at the serine residue S536 (p-NF- κ Bp65 S536) in $Panx1^{-/-}$ mice ($p \leq 0.0001$) (Fig. 5a; Supplementary Fig. 1a). In the BDL group, the number of CD68⁺ cells were increased in $Panx1^{-/-}$ mice ($p \leq 0.05$) (Fig. 5b). However, these animals presented no differences of p-NF- κ Bp65 S536 protein levels (Fig. 5b; Supplementary Fig. 1b).

$Panx1$ channels are known to modulate Nalp3 inflammasome activation in hepatic macrophages (Kim et al. 2015). In addition to the reduced protein levels of p-NF- κ Bp65

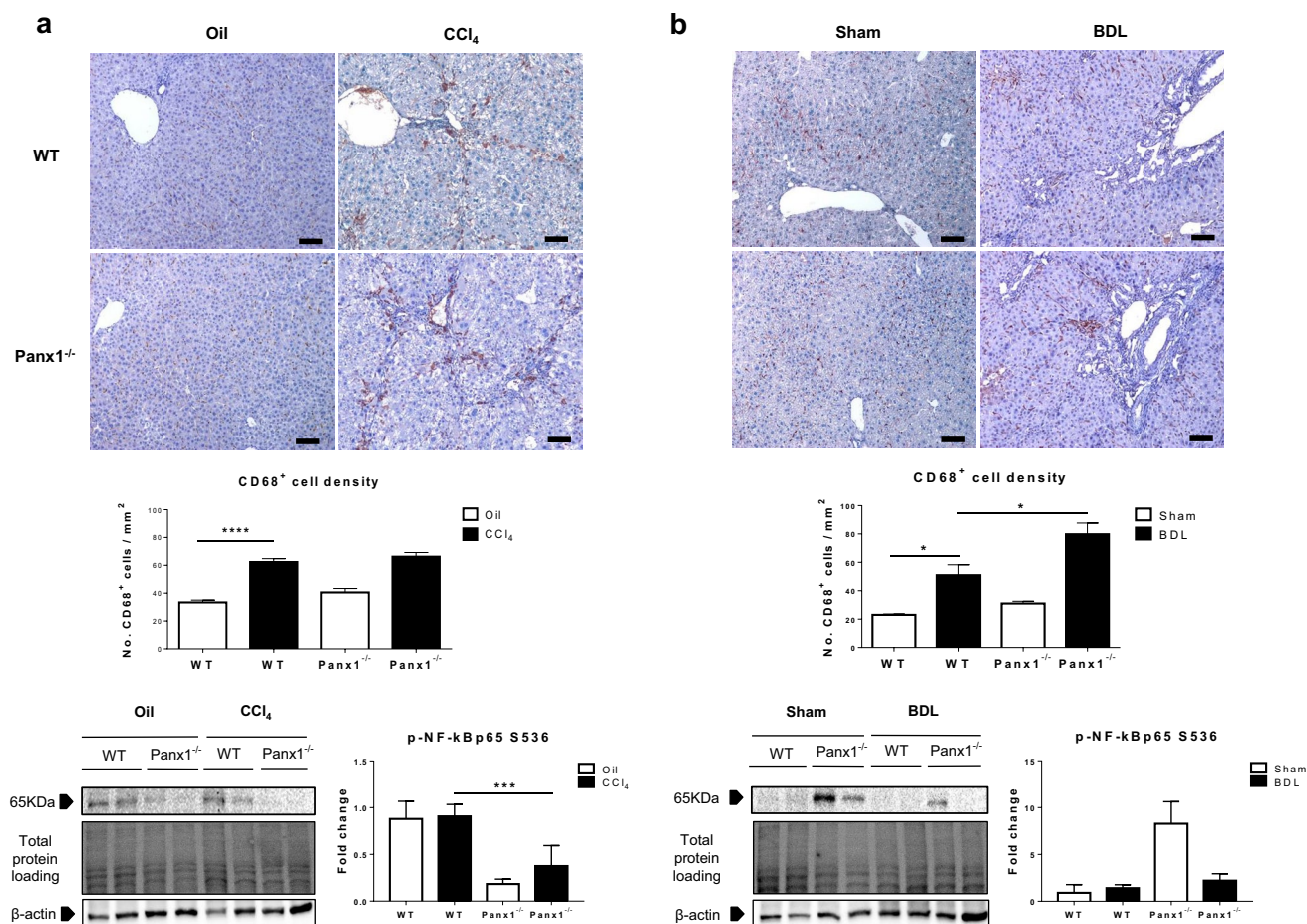


Fig. 5 Effect of genetic $Panx1$ deficiency on inflammation in liver fibrosis. WT and $Panx1^{-/-}$ mice were administered 20% CCl₄ ip at a gradually increased dose for 8 weeks or subjected to BDL for 20 days. Representative images for the calculation of hepatic CD68⁺ cell density ($n = 5$) and example of blot membranes for the determination of p-NF- κ Bp65 S536 protein levels ($n = 9-15$) in **a** the CCl₄

model and **b** the BDL model. Results were analyzed by one-way ANOVA followed by post hoc tests using Bonferroni correction and with Kruskal–Wallis test followed by post hoc tests using Dunn’s correction in case of the p-NF- κ Bp65 S536. Data were expressed as means \pm SEM or median \pm interquartile ($*p \leq 0.05$; $***p \leq 0.001$; $****p \leq 0.0001$). Scale bar represents 20 μ m

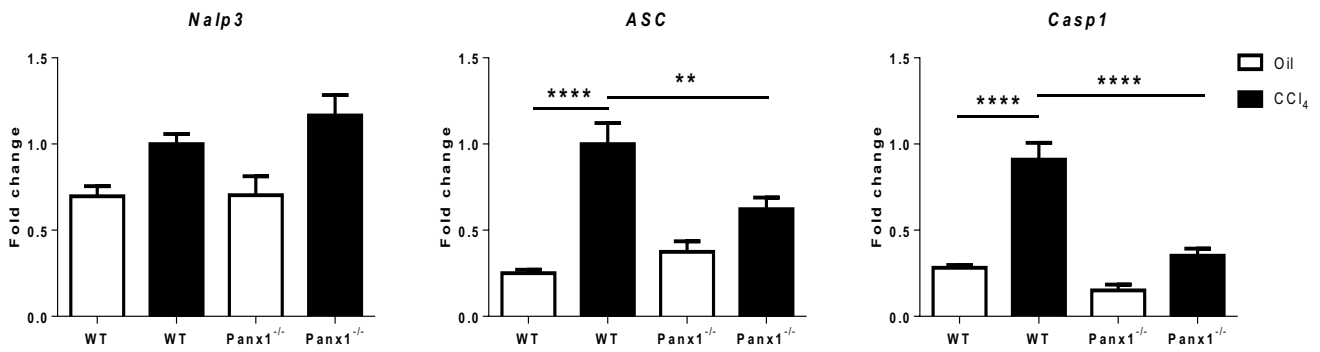


Fig. 6 Effect of genetic Panx1 deficiency on the Nalp3 inflammatory components in liver fibrosis. WT and Panx1^{-/-} mice (n=10) were administered 20% CCl₄ ip at a gradually increased dose for 8

weeks. Results were analyzed by one-way ANOVA followed by post hoc tests using Bonferroni correction. Data were expressed as means ± SEM (**p ≤ 0.01; ****p ≤ 0.0001)

Fig. 7 Antibody array map with the inflammatory proteins (BLC, B lymphocyte chemoattractant; CD30L, tumor necrosis factor ligand superfamily member 8; Eotx, eotaxin; Frck, fractalkine, GCSF, granulocyte colony-stimulating factor; GM-CSF, granulocyte-macrophage colony-stimulating factor; IFN γ , interferon gamma; IL1 α /1 β /2/7/4/6/9/10/12/13/17, interleukin 1 alpha/1 beta/2/7/4/6/9/10/12/13/17; ITAC, interferon-inducible T-cell alpha chemoattractant; KC, growth-regulated alpha protein; Lept, leptin; LIX, lipopolysaccharide-induced CXC chemokine; Lymp, lymphotactin; MCP-1, monocyte chemoattractant protein 1; MCSF, macrophage colony-stimulating factor; MIG, monokine induced by gamma interferon; MIP1 α / γ , macrophage inflammatory protein 1 alpha/gamma; Neg, negative; Pos, positive; RNTS, rantes; SDF-1, stromal cell-derived factor 1; sTNF RI/II, soluble TNF receptor 1/2; TCA-3, T-cell activation protein 3; TECK, thymus-expressed chemokine; TIMP-1/-2, tissue inhibitor of metalloproteinase-1/-2; TNF α , tumor necrosis factor alpha)

GCSF	GCSF	IL12 p70	IL12 p70	MIP1 γ	MIP1 γ	Pos	Pos
Frck	Frck	IL12 p40/p70	IL12 p40/p70	MIP1 α	MIP1 α	Blank	Blank
Fas	Fas	IL10	IL10	MIG	MIG	Blank	Blank
Eotx2	Eotx2	IL9	IL9	MCSF	MCSF	sTNF RII	sTNF RII
Eotx	Eotx	IL6	IL6	MCP-1	MCP-1	sTNF RI	sTNF RI
CD30L	CD30L	IL4	IL4	Lymp	Lymp	TNF α	TNF α
BLC	BLC	IL7	IL7	LIX	LIX	TIMP-2	TIMP-2
Blank	Blank	IL2	IL2	Lept	Lept	TIMP-1	TIMP-1
Neg	Neg	IL1 β	IL1 β	KC	KC	TECK	TECK
Neg	Neg	IL1 α	IL1 α	ITAC	ITAC	TCA-3	TCA-3
Pos	Pos	IFN γ	IFN γ	IL17	IL17	SDF-1	SDF-1
Pos	Pos	GM-CSF	GM-CSF	IL13	IL13	RNTS	RNTS

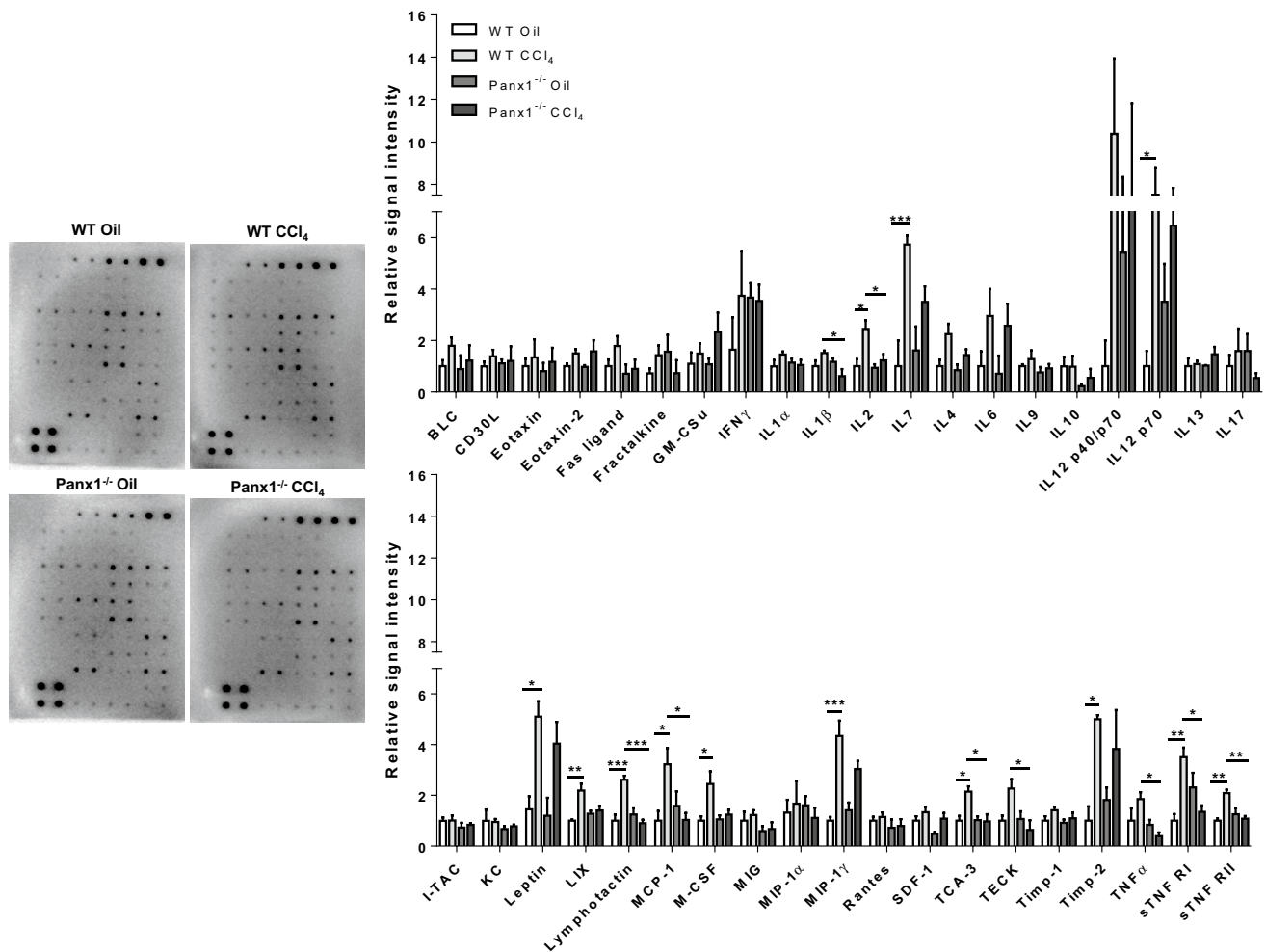


Fig. 8 Effect of genetic Panx1 deficiency on inflammatory proteins in chemically-induced liver fibrosis. WT and Panx1^{-/-} mice ($n=4$) were administered 20% CCl₄ ip at a gradually increased dose for 8 weeks. Representative antibody array membranes from liver tissue extract corresponded to WT and Panx1^{-/-} treated with oil or CCl₄.

Data were analyzed by densitometry analysis. Then, background was subtracted and results were normalized against the average of positive control. Results were analyzed by one-way ANOVA followed by post hoc tests using Bonferroni correction. Data were expressed as means \pm SEM (* $p \leq 0.05$; ** $p \leq 0.01$; *** $p \leq 0.001$)

S536, the RNA levels of Nalp3 inflammasome components apoptosis-associated speck-like protein containing a C-terminal caspase-recruitment domain (ASC) ($p \leq 0.01$) and caspase 1 (Casp1) ($p \leq 0.0001$) were indeed downregulated in CCl₄-treated Panx1^{-/-} mice (Fig. 6). Thereafter, 40 proteins involved in inflammation were evaluated to determine the effect of Panx1^{-/-} in liver fibrosis (Fig. 7). In the CCl₄ model, lowered protein levels of IL1 β ($p \leq 0.05$), IL2 ($p \leq 0.05$), lymphotactin ($p \leq 0.001$), monocyte chemoattractant protein 1 (MCP-1) ($p \leq 0.05$), T-cell activation protein 3 (TCA-3) ($p \leq 0.05$), thymus-expressed chemokine (TECK) ($p \leq 0.05$), TNF α ($p \leq 0.05$), soluble TNF receptor 1 (sTNF-RI) ($p \leq 0.05$) and sTNF-RII ($p \leq 0.01$) were observed in the Panx1^{-/-} mice (Fig. 8). In the BDL group, only the macrophage protein 1 gamma (MIP1 γ) was increased due to Panx1^{-/-} (Fig. 9). To further characterize

the immune response, a series of stainings against typical immune cell markers were performed. In the CCl₄ model, the immune cell population was mainly represented by the CD11b⁺ and Ly6c⁺ cells, usually expressed by the inflammatory monocyte subset considered as precursors of tissue macrophages. Both markers were observed in areas surrounding the scar tissue of WT and Panx1^{-/-} mice treated with CCl₄ (Fig. 10). In addition, only small amounts of neutrophils (Ly6g⁺ cells) and scarce T-lymphocytes (CD3⁺ cells) were observed in the fibrotic liver tissue of WT and Panx1^{-/-} mice. In the BDL group, CD11b⁺, Ly6c⁺ and Ly6g⁺ cells were located in the portal and necrotic areas of liver from WT and Panx1^{-/-} mice (Fig. 11). In addition, CD11b⁺ and Ly6c⁺ cell infiltration within the parenchyma of the BDL-subjected Panx1^{-/-} cohort was observed (Fig. 11).

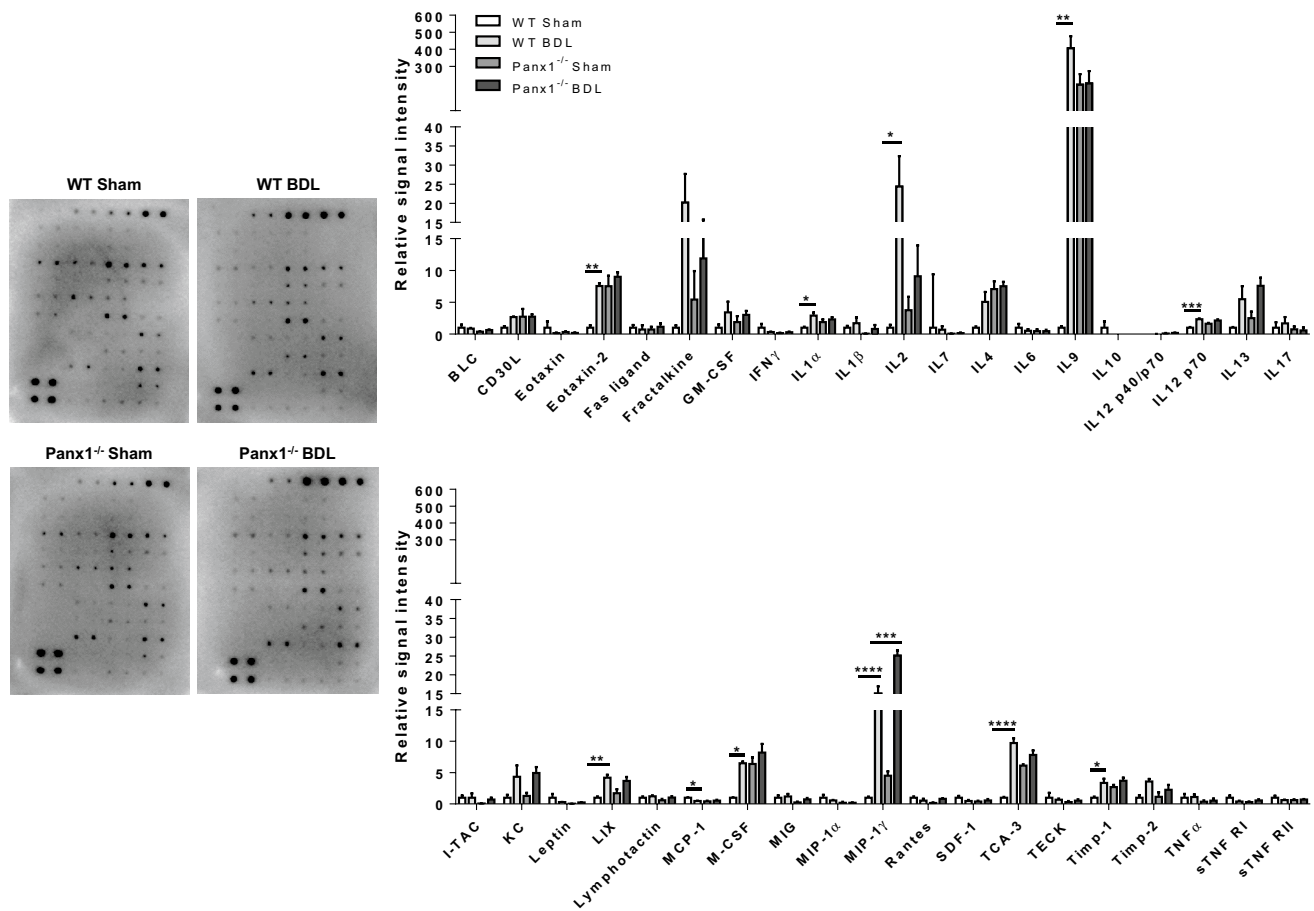


Fig. 9 Effect of genetic Panx1 deficiency on inflammatory proteins in surgically-induced liver fibrosis. WT and Panx1^{-/-} mice ($n=4$) were subjected to BDL for 20 days. Representative antibody array membranes from liver tissue extract corresponded to WT and Panx1^{-/-} subjected to sham or BDL. Data were analyzed by densitometry

analysis. Then, background was subtracted and results were normalized against the average of positive control. Results were analyzed by one-way ANOVA followed by post hoc tests using Bonferroni correction. Data were expressed as means \pm SEM (* $p \leq 0.05$; ** $p \leq 0.01$; *** $p \leq 0.001$; **** $p \leq 0.0001$)

T cells stained for CD3 were restricted to the liver portal areas of BDL-subjected WT and Panx1^{-/-} animals.

Effects of genetic Panx1 deficiency on regenerative capacity in liver fibrosis

Hepatocyte proliferation is critical to ensure the healing process after liver injury. Accordingly, the regenerative capacity was determined through staining and counting of Ki-67⁺ cells in liver tissue. Untreated WT and Panx1^{-/-} mice seemed to rarely express Ki-67. In the CCl₄ group, but not in the BDL cohort, Panx1^{-/-} animals showed less Ki-67⁺ hepatocytes ($p \leq 0.05$) (Fig. 12a, b). It is well-known that bile duct blockage leads to the proliferation of cholangiocytes, which triggers bile duct hyperplasia. In this respect, the number of Ki-67⁺ cholangiocytes upon BDL was equal among all experimental groups (Fig. 12b).

Effect of genetic Panx1 deficiency on the liver transcriptome in liver fibrosis

To shed more light onto the involvement of Panx1 signaling pathways in the fibrotic response, global gene expression profiles were studied in WT and Panx1^{-/-} whether or not treated with CCl₄ or subjected to BDL. CCl₄ treatment in WT and Panx1^{-/-} resulted in 223 and 192 differentially modulated genes, respectively, with at least twofold change and $p < 0.05$ compared to untreated WT animals. When compared, 3 clusters of genes were identified, including: (1) 103 genes specifically modulated due to CCl₄ treatment in the WT genetic background (Supplementary Table 1), (2) 120 regulated genes resulting from the CCl₄ treatment (Supplementary Table 2) and (3) 72 genes associated with the CCl₄ treatment in the Panx1^{-/-} genetic background (Table 2) (Fig. 13a). The most prominent reduction in the networks within the CCl₄ treatment cluster due to Panx1^{-/-} was centered on a plethora of genes related to cell cycle, fibrotic and

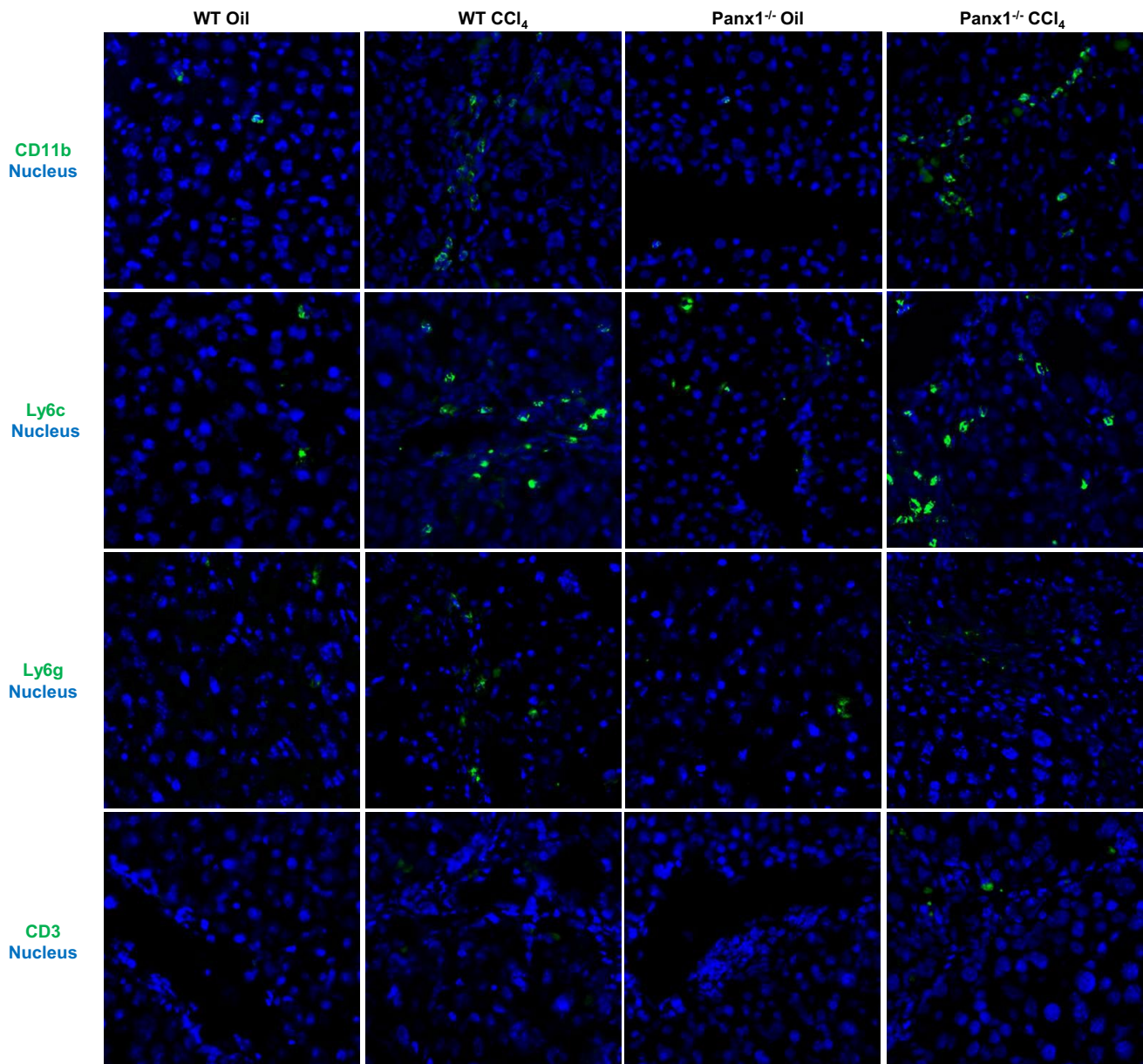


Fig. 10 Effect of genetic Panx1 deficiency on immune cell infiltration in chemically-induced liver fibrosis. WT and Panx1^{-/-} mice ($n=3$) were administered 20% CCl₄ ip at a gradually increased dose for 8 weeks. Representative images from CD11b, Ly6c, Ly6g and CD3 immune markers

immune responses, metabolism, and oxidation–reduction and epoxygenase activities. Among those, pro-fibrogenic genes required for pathological extracellular matrix formation as well as genes involved in muscle contraction were strongly downregulated. In addition, in the Panx1^{-/-} genetic background cluster, suppressed expression of genes involved in the fibrotic response was observed, which reinforces the observed reduced collagen content and HSC activation in CCl₄-treated Panx1^{-/-} animals. Downregulated immune genes related to the Toll-like receptor (TLR) signaling, leukocyte migration and chemotaxis. Effects on the TLR signaling pathway were also confirmed by RT-qPCR analysis

of the genes dectin-1 (*Clec7a*), lipopolysaccharide-binding protein (*Lbp*) and the lymphocyte antigen 96 (*Ly96*). Expression of *Clec7a* ($p \leq 0.0001$) and *Lbp* ($p \leq 0.01$) was significantly reduced, while no changes in *Ly96* were found in the CCl₄-treated Panx1^{-/-} mice (Fig. 13b). This is in line with the observed reduced protein levels of p-NF-κBp65 S536. Several other genes encoding mediators of immunity, metabolism and transportation were also negatively affected (Table 2).

Likewise, 3 gene clusters could be identified following BDL, including: (1) 137 genes modulated due to the BDL procedure in the WT genetic background (Supplementary

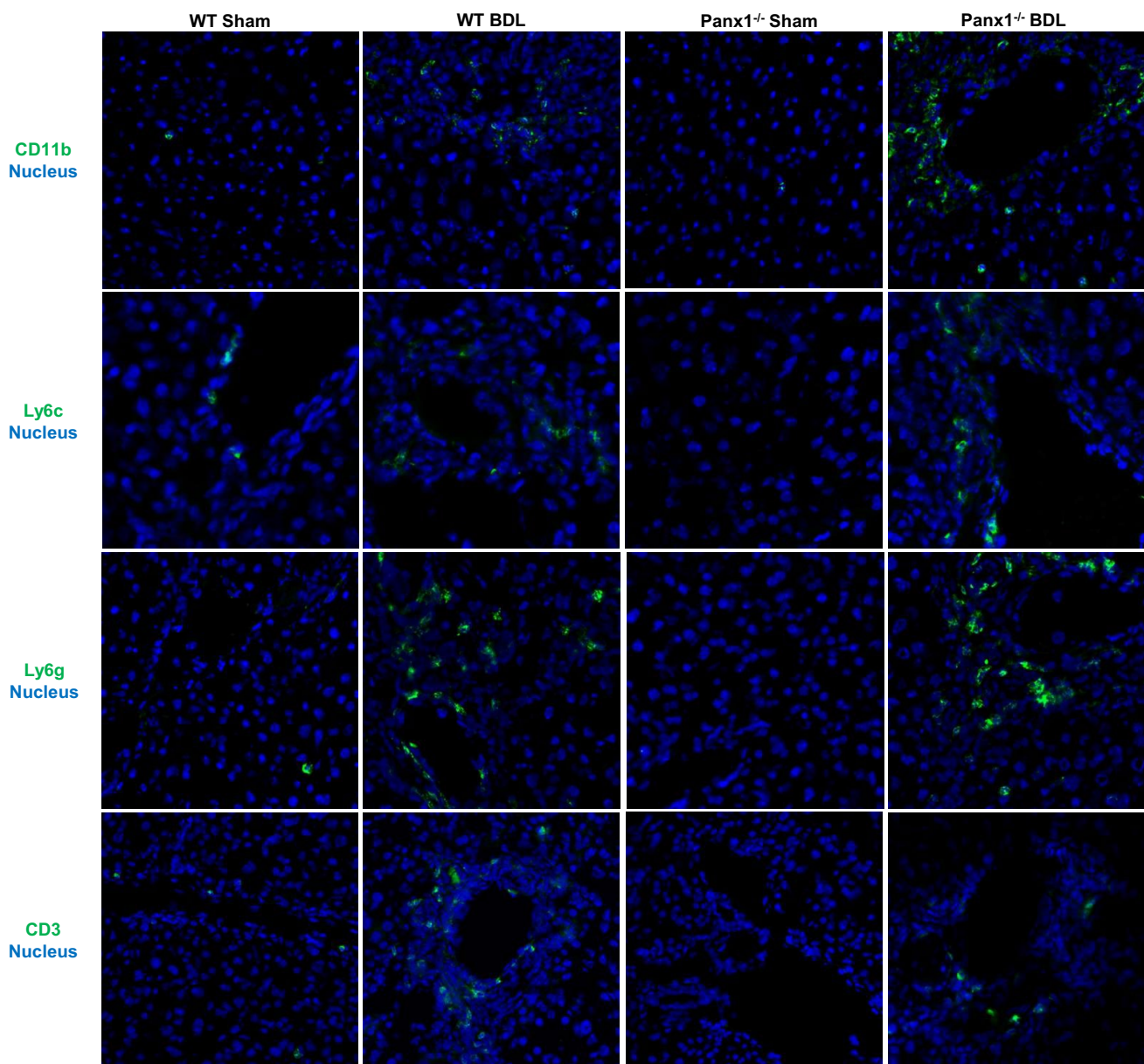


Fig. 11 Effect of genetic Panx1 deficiency on immune cell infiltration in surgically induced liver fibrosis. WT and Panx1^{-/-} mice ($n=3$) were subjected to BDL for 20 days. Representative images from CD11b, Ly6c, Ly6g and CD3 immune markers

Table 3), (2) 341 genes altered through the BDL procedure (Supplementary Table 4), and (3) 39 genes associated with BDL procedure in Panx1^{-/-} mice (Table 3) with at least twofold change and $p < 0.05$ (Fig. 14a). Although only minimum differences in the overall gene modulation ontology were observed within the BDL cluster, several genes related to the immune response were markedly downregulated as a consequence of genetic Panx1 ablation. Downregulated genes related to cell adhesion, activation, migration functions and TLR signaling. In contrast, genes critical for chemotaxis, TLR4 signaling, leukocyte migration, platelet activation and neutrophil degranulation were upregulated.

Nevertheless, RT-qPCR analysis revealed no modification in S100 calcium-binding protein A9 (*S100a9*) levels in BDL-subjected Panx1^{-/-} mice (Fig. 14b). The major upregulated pathways in BDL-subjected Panx1^{-/-} mice were related to immune responses (Table 3). Out of them, chemokine ligand 14 (*Cxcl14*) was evaluated by RT-qPCR, resulting in a lack of modulation in BDL-subjected Panx1^{-/-} mice (Fig. 14b). This supports the elevated numbers of macrophages observed in BDL-subjected Panx1^{-/-} mice.

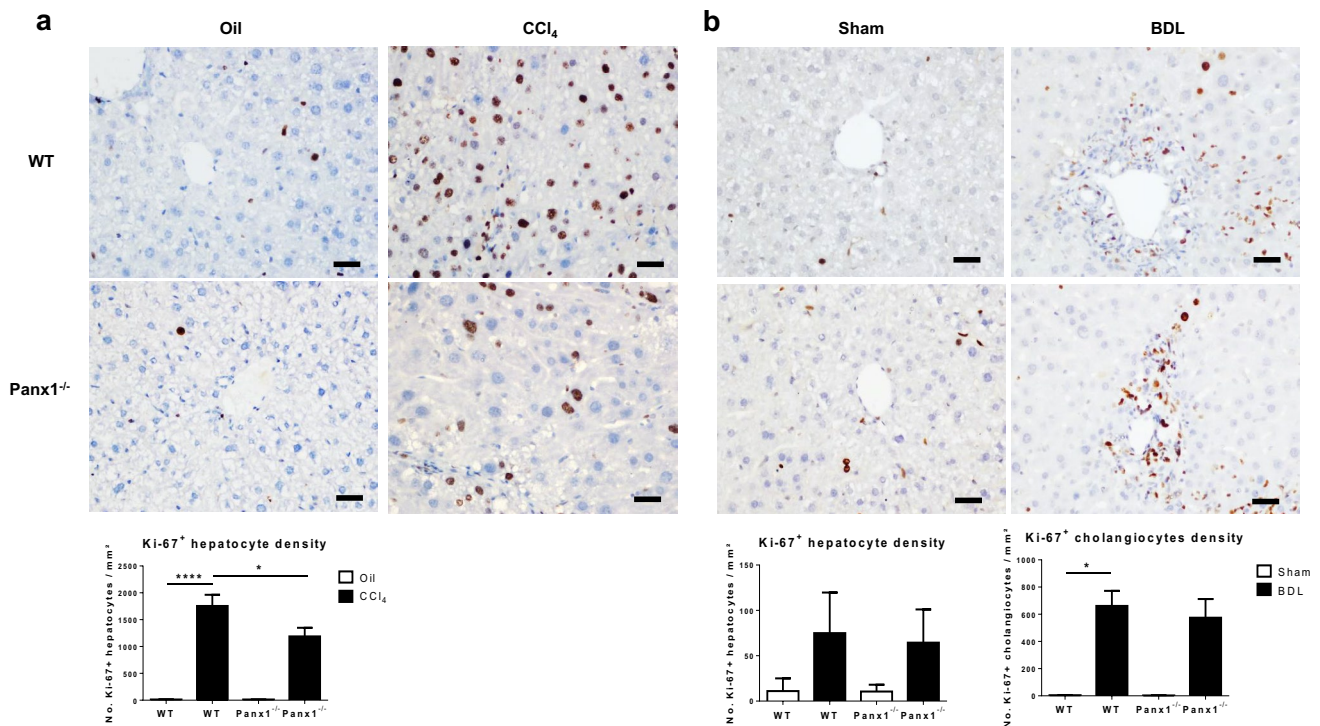


Fig. 12 Effect of genetic Panx1 deficiency on regenerative capacity in liver fibrosis. WT and Panx1^{-/-} mice ($n=5$) were administered 20% CCl₄ ip at a gradually increased dose for 8 weeks or subjected to BDL for 20 days. Ki-67⁺ cell density in **a** the CCl₄ model and **b** the BDL model. Results were analyzed by one-way ANOVA followed by

post hoc tests using Bonferroni correction and with Kruskal–Wallis test followed by post hoc tests using Dunn's correction in case of the Ki-67⁺ hepatocytes and cholangiocytes within the BDL model. Data were expressed as means \pm SEM or median \pm interquartile ($*p \leq 0.05$; $***p \leq 0.0001$). Scale bar represents 20 μ m

Discussion

Transdifferentiation of quiescent into activated HSCs constitutes an important feature in the progression of liver fibrosis. Despite the wealth of knowledge regarding the involvement of signaling pathways to this process, the participation of communication mediated by Panx1 channels has been poorly documented thus far. In this regard, this study showed increased expression of Panx1 in mouse liver following CCl₄ treatment or BDL surgery, which has also been found in experimental models of non-alcoholic steatohepatitis (Csak et al. 2011), acute liver failure (Maes et al. 2017) and ischemia/reperfusion injury (Kim et al. 2015). Accordingly, CCl₄-treated Panx1^{-/-} mice seem more protected as evidenced by the reduced fibrotic response, pro-inflammatory signaling and hepatic regeneration. By contrast, BDL-subjected Panx1^{-/-} mice showed a marked hepatocellular injury and increased antioxidant enzyme activity with a predominant immune response.

Panx1 channels have been described to play a role in inflammatory mechanisms in liver disease either by the recruitment of leukocytes or through the activation of the

Nalp3 inflammasome (Csak et al. 2011; Kim et al. 2015; Maes et al. 2017; Xiao et al. 2015). Indeed, Nalp3 inflammasome activation in myeloid-derived cells triggers liver inflammation, leukocyte infiltration, pro-inflammatory macrophage recruitment and activation of fibrogenic pathways (Wree et al. 2014). In this respect, CCl₄-treated WT and Panx1^{-/-} showed an immune cell population mainly characterized by the presence of CD11b⁺ and Ly6c⁺ cells. In fact, unmodified CD68⁺ macrophage numbers, but decreased hepatic Nalp3 inflammasome component expression, lowered protein levels of p-NF- κ Bp65 S536 and reduced amounts of a number of inflammatory proteins were found. Among those, a lowered production of the inflammasome-dependent IL1 β was observed as well as decreased protein levels of TNF α and its respective receptors, sTNF-RI and -RII. This suggests that genetic Panx1 deletion interferes with signaling pathways that contribute to IL1 β and TNF α secretion, which in turn affects the survival of activated HSCs through NF- κ B activation (Pradere et al. 2013). Consequently, pro-inflammatory proteins released by activated HSCs, macrophages or involved in HSC recruitment, such as MCP-1 or TECK, were negatively affected. In addition to the reduced survival of activated HSC, decreased cytokine secretion influences the

Table 2 Gene modulation by CCl₄ treatment in Panx1^{-/-} genetic background

Functional gene class	Gene symbol	Gene description	Panx1 ^{-/-} -CCl ₄ vs WT-Oil		
			Fold change	<i>p</i> value	
Cell cycle	<i>Aurka</i>	Aurora kinase A	2.05	0.000221	
	<i>Ccnd1</i>	Cyclin D1	2.18	0.000136	
Cell death	<i>Hist1h1a</i>	Histone cluster 1, H1a	2.03	0.000695	
	<i>Osgin1</i>	Oxidative stress-induced growth inhibitor 1	- 2.29	0.001804	
Fibrotic response	<i>Avpr1a</i>	Arginine vasopressin receptor 1A	- 2.38	0.001408	
	<i>Inhbc</i>	Inhibin beta-C	- 2.05	0.000368	
	<i>Nrp1</i>	Neuropilin 1	- 2.06	0.001032	
Immune response	<i>Cd5l</i>	CD5 antigen-like	2.12	0.006417	
	<i>Cd59a</i>	CD59a antigen	- 2.26	0.000149	
	<i>Ceacam1</i>	Carcinoembryonic antigen-related cell adhesion molecule 1	- 2.06	0.000299	
	<i>Colec12</i>	Collectin sub-family member 12	- 2.02	0.001828	
	<i>Lbp</i>	Lipopolysaccharide-binding protein	- 2.24	0.000163	
	<i>Lrg1</i>	Leucine-rich alpha-2-glycoprotein 1	- 2.16	0.002557	
	<i>Ly96</i>	Lymphocyte antigen 96	- 2.23	0.009796	
	<i>S100a9</i>	S100 calcium-binding protein A9 (calgranulin B)	2.14	0.000362	
	<i>Saa4</i>	Serum amyloid A 4	- 3.03	0.003026	
	Metabolism	<i>Abhd14b</i>	Abhydrolase domain-containing 14b	- 2.04	0.000124
<i>Akr1e1</i>		Aldo-keto reductase family 1, member E1	8.5	0.000093	
<i>Ces3b</i>		Carboxylesterase 3B	- 2.41	0.003169	
<i>Coq5</i>		Coenzyme Q5 methyltransferase	- 2.22	0.000179	
<i>Enho</i>		Energy homeostasis associated	- 2.17	0.000197	
<i>Fgl1</i>		Fibrinogen-like protein 1	- 2.04	0.0269	
<i>Mocs1</i>		Molybdenum cofactor synthesis 1	- 2.6	0.000084	
<i>Papss1</i>		3-phosphoadenosine 5-phosphosulfate synthase 1; 3'-phosphoadenosine 5'-phosphosulfate synthase 1; 3'-phosphoadenosine 5'-phosphosulfate synthase 1	- 2.07	0.00667	
Oxidation-reduction and epoxygenase activity		<i>Cmah</i>	Cytidine monophospho- <i>N</i> -acetylneuraminic acid hydroxylase	- 2.05	0.003293
		<i>Cyp2c40</i>	Cytochrome P450, family 2, subfamily c, polypeptide 40	- 2.02	0.01303
	<i>Cyp4a32</i>	Cytochrome P450, family 4, subfamily a, polypeptide 32	- 2.42	0.02169	
	<i>Cyp8b1</i>	Cytochrome P450, family 8, subfamily b, polypeptide 1	- 4.69	0.000675	
	<i>Ldhd</i>	Lactate dehydrogenase D	- 2.12	0.000046	
Transporter activity	<i>Abcb1a</i>	ATP-binding cassette, sub-family B (MDR/TAP), member 1A	2.27	0.002479	
	<i>Slc13a3</i>	Solute carrier family 13 (sodium-dependent dicarboxylate transporter), member 3	- 2.02	0.002296	
	<i>Slc16a10</i>	Solute carrier family 16 (monocarboxylic acid transporters), member 10	- 2.53	0.001261	
	<i>Slc19a2</i>	Solute carrier family 19 (thiamine transporter), member 2	- 2.15	0.00055	
	<i>Slc35e3</i>	Solute carrier family 35, member E3	- 2.06	0.001345	
	<i>Slco2a1</i>	Solute carrier organic anion transporter family, member 2a1	- 2.06	0.000034	

Table 2 (continued)

Functional gene class	Gene symbol	Gene description	Panx1 ^{-/-} -CCl ₄ vs WT-Oil		
			Fold change	p value	
Miscellaneous	<i>Derl3</i>	Der1-like domain family, member 3	- 2.24	0.031476	
	<i>Dnajb11</i>	DnaJ (Hsp40) homolog, subfamily B, member 11	- 2.01	0.019102	
	<i>Dpy19l3</i>	Dpy-19-like 3 (C. elegans)	- 2.5	0.00003	
	<i>Mettl20</i>	Methyltransferase like 20	- 2.03	0.017972	
	<i>Nr1d1</i>	Nuclear receptor subfamily 1, group D, member 1	- 2.05	0.00128	
	<i>Paqr9</i>	Progesterin and adipoQ receptor family member IX	- 2.17	0.015826	
	<i>Pdia4; Mir704</i>	Protein disulfide isomerase associated 4; microRNA 704	- 2.03	0.022389	
	<i>Pstpip2</i>	Proline-serine-threonine phosphatase-interacting protein 2	- 2.25	0.006075	
	<i>Rmrp</i>	RNA component of mitochondrial RNAase P	2.13	0.001084	
	<i>Rtp3</i>	Receptor transporter protein 3	- 2.39	0.002252	
	<i>Sdf2l1</i>	Stromal cell-derived factor 2-like 1	- 2.03	0.001343	
	<i>Tff3</i>	Trefoil factor 3, intestinal	- 2.16	0.030926	
	<i>Tuba4a</i>	Tubulin, alpha 4A	- 2.25	0.004131	
	<i>Vps33b</i>	Vacuolar protein sorting 33B (yeast)	- 2.03	0.000144	
	Not determined	<i>8430408G22Rik</i>	RIKEN cDNA 8430408G22 gene	- 2.19	0.001611
		<i>Creld2</i>	Cysteine-rich with EGF-like domains 2	- 5.98	0.018213
<i>Drr1</i>		Developmentally regulated repeat element-containing transcript 1	2.13	0.018309	
<i>Mir292b</i>		microRNA 292b	- 2.48	0.000564	
<i>Mir297-1</i>		microRNA 297-1	2.49	0.002843	
<i>Mir466f-3</i>		microRNA 466f-3	2.45	0.039387	
<i>Mir5111</i>		microRNA 5111 (Mir5111), microRNA	2.12	0.002563	
<i>Mir5124a; Mir5124</i>		microRNA 5124a; microRNA 5124	2.24	0.034207	
<i>Mir5125</i>		microRNA 5125	2.86	0.006299	
<i>mt-Ts2; mt-Tl2</i>		Mitochondrially encoded tRNA serine 2; mitochondrially encoded tRNA leucine 2	5.06	0.044986	
<i>Pkhd1l1</i>		Polycystic kidney and hepatic disease 1-like 1	2.02	0.00392	
<i>Rnu12</i>		RNA U12, small nuclear	2.05	0.000569	
<i>Rnu3a</i>		U3A small nuclear RNA	2.21	0.00131	
<i>Rps24-ps3</i>		Ribosomal protein S24, pseudogene 3	- 2.03	0.028906	
<i>Scarna6</i>		Small Cajal body-specific RNA 6	2.28	0.000036	
<i>Snora34</i>		Small nucleolar RNA, H/ACA box 34	3	0.03671	
<i>Snora69</i>		Small nucleolar RNA, H/ACA box 69	2.57	0.025828	
<i>Snora75</i>		Small nucleolar RNA, H/ACA box 75	2.68	0.012425	
<i>Snord118</i>		Small nucleolar RNA, C/D box 118	2.22	0.000584	
<i>Snord93</i>		Small nucleolar RNA, C/D box 93	4.11	0.004554	
<i>Them7</i>		Thioesterase superfamily member 7	- 2.53	0.000797	
<i>Tmem19</i>		Transmembrane protein 19	- 2.04	0.020126	
<i>Tmem254b; Tmem254c; Tmem254a</i>		Transmembrane protein 254b; transmembrane protein 254c; transmembrane protein 254a	- 6.9	0.0000003	

occurrence of diminished hepatic injury (Seki and Schwabe 2015). Indeed, the lowed hepatic proliferation might constitute a compensatory effect. Other mechanisms involved in the apoptotic cell death of activated HSCs include excessive oxidative stress (Dunning et al. 2013). CCl₄-treated Panx1^{-/-} mice accumulate hydrogen peroxide because of SOD overactivation and the absence of modulation of the

hydrogen peroxide-scavengers GPx and catalase. This may represent an alternative mechanism that could contribute to the decreased activated HSCs levels. In contrast, this effect may not apply to the BDL-subjected mice, since increased GPx activity was observed. Although no direct association between Panx1 and SOD or GPx has been reported thus far, hydrogen peroxide is known to transiently affect Panx1

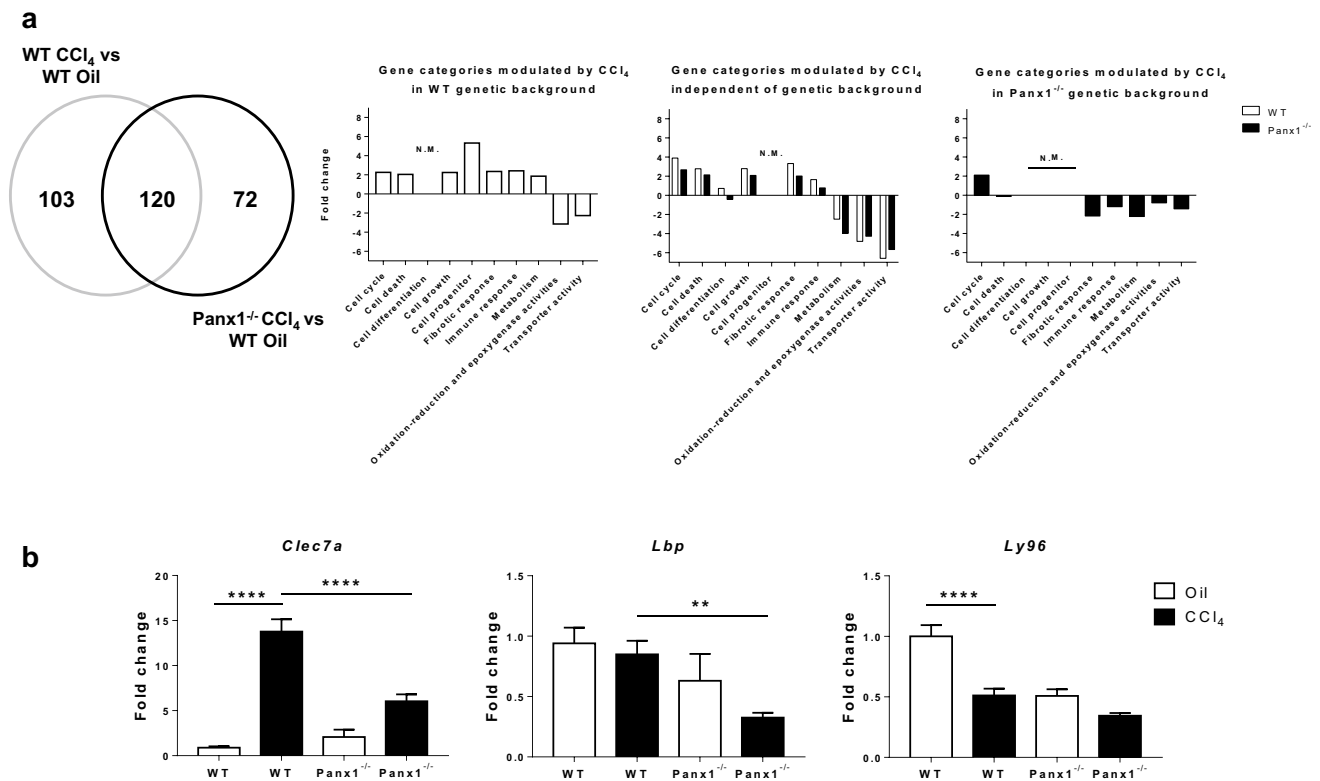


Fig. 13 Panx1 deficiency effect in the liver transcriptome in liver fibrosis. WT and Panx1^{-/-} mice ($n=5$) administered 20% CCl₄ ip at a gradually increased dose for 8 weeks. **a** Gene ontology of the different clusters of modulated genes expressed as the average of the fold change from genes with at least twofold difference and $p < 0.05$

and **b** RT-qPCR analysis from genes corresponded to the categories: CCl₄ independent of genetic background or CCl₄ in Panx1^{-/-} genetic background. Results were analyzed by one-way ANOVA followed by post hoc tests using Bonferroni correction. Data were expressed as means \pm SEM (** $p \leq 0.01$; **** $p \leq 0.0001$). N.M. not modulated

channel function (Krick et al. 2016). This points to modulation of the oxidative stress scavengers as being a secondary effect to genetic Panx1 ablation. On the other hand, the Panx1^{-/-} potentiates the number of macrophages and the protein levels of MIP1 γ , but not NF- κ B activation, upon BDL surgery. MIP1 γ is mainly produced by macrophages and functions as a cell survival factor and plays a role in the recruitment of myeloid progenitor cells to mediate in a metastasis-promoting effect (Hara et al. 1995; Yan et al. 2015). It is uncertain whether these changes are induced by the accumulation of bile acids in macrophages. Recent data support that the farnesoid X receptor regulates bile acid-induced Nalp3 inflammasome activation in macrophages (Hao et al. 2017). Although ATP synergizes with bile acids to activate Nalp3 (Hao et al. 2017), selective inhibition of Panx1 does not alter extracellular ATP concentrations in pancreatic cells (Kowal et al. 2015), which could point to Panx1-independent activation of Nalp3 under these conditions. In fact, this was also evidenced by the lack of modification in the protein levels of IL1 β . Alternatively, other immune cellular subsets clustered within the CD3⁺, CD11b⁺, Ly6c⁺ or Ly6g⁺ cell population were identified in

the BDL-subjected WT and Panx1^{-/-} cohorts. This substantiates that in addition to macrophages, T cells and neutrophils might contribute to the deterioration of the cholestatic liver. In experimental chronic cholestasis, however, neutrophils lack to participate in the wound healing response either in the promotion of hepatic damage (Moles et al. 2014; Saito et al. 2003) and are guided to the injured liver through a mechanism mediated by CXCL2 (Moles et al. 2014). This mechanism could explain why, in contrast to previous studies (Bao et al. 2013), Panx1 channels are not required for the fine-tuning of neutrophil migration in the BDL model. These changes indicate a shift towards an exacerbated immune reaction independently of Nalp3 inflammasome activation and neutrophil infiltration, but mainly governed by the action of macrophages, which may substantiate the maintenance of activated HSCs as well as the pronounced hepatic injury.

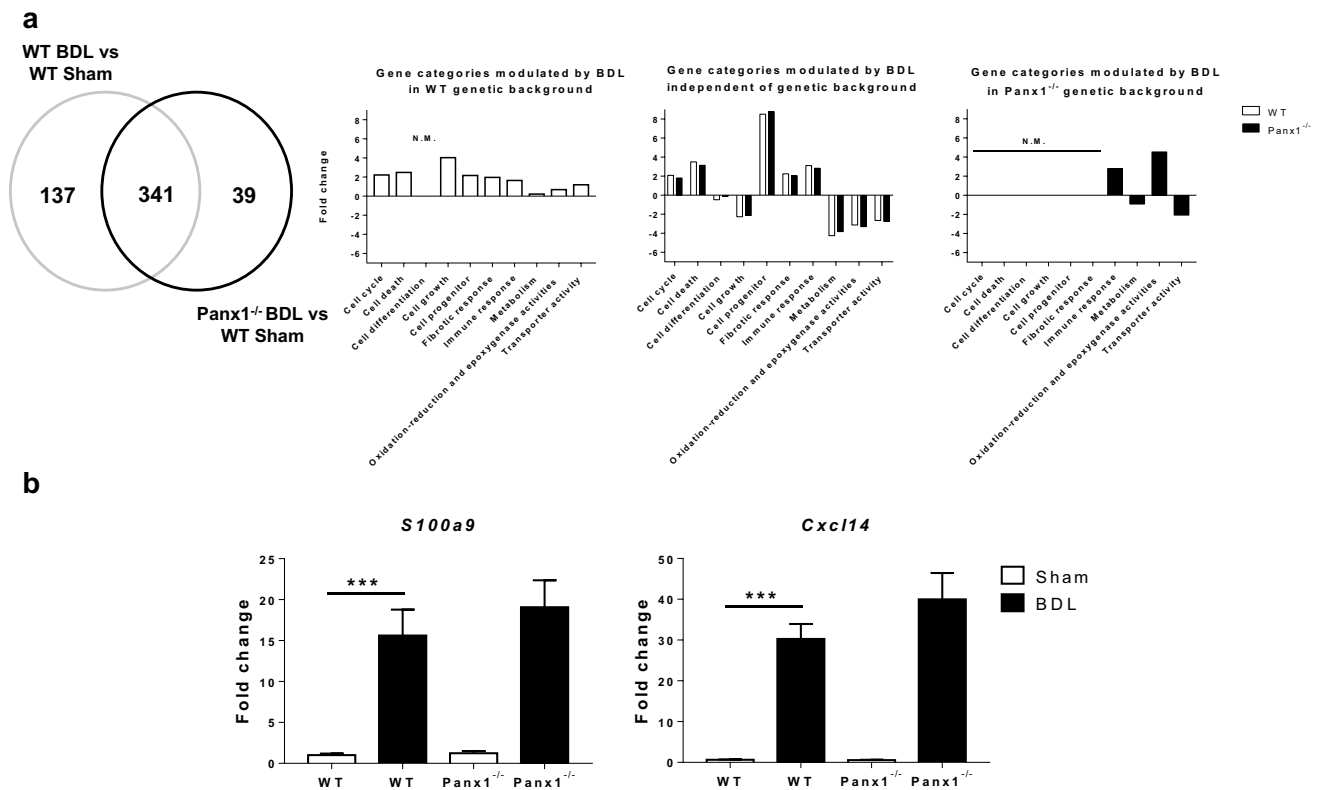
Global gene expression profiling was performed to investigate the molecular mechanisms driven by Panx1 signaling in CCl₄-treated and BDL-subjected mice. Several genes associated with fibrotic and immune responses were downregulated or negatively modulated in the CCl₄-treated Panx1^{-/-} animals. Among those, the *Clec7a*, *Lbp* and *Ly96*

Table 3 Gene modulation by the BDL procedure in *Panx1*^{-/-} genetic background

Functional gene class	Gene symbol	Gene description	Panx1 ^{-/-} -BDL vs WT-Sham	
			Fold change	<i>p</i> value
Fibrotic response	<i>S100a6</i>	S100 calcium-binding protein A6 (calcyclin)	2.52	0.0002
Immune response	<i>Cxcl14</i>	Chemokine (C-X-C motif) ligand 14	2.23	0.00001
	<i>Hp</i>	Haptoglobin	2.01	0.0004
	<i>Plscr1</i>	Phospholipid scramblase 1	2.20	0.0000001
	<i>Rnf125</i>	Ring finger protein 125	2.08	0.01
	<i>Saa2</i>	Serum amyloid A 2	5.70	0.03
	<i>Ephx2</i>	Epoxide hydrolase 2, cytoplasmic	- 2.08	0.0002
Metabolism	<i>Golm1</i>	Golgi membrane protein 1	2.34	0.00001
	<i>Gsta4</i>	Glutathione S-transferase, alpha 4	2.14	0.0004
	<i>Hsd3b2</i>	Hydroxy-delta-5-steroid dehydrogenase, 3 beta- and steroid delta-isomerase 2	- 2.05	0.001
	<i>Pah</i>	Phenylalanine hydroxylase	- 2.10	0.0003
	<i>Thrsp</i>	Thyroid hormone responsive	- 2.61	0.005
	<i>Upp2</i>	Uridine phosphorylase 2	- 2.02	0.001
	Oxidation–reduction and epoxygenase activities	<i>Akr1e1</i>	Aldo–keto reductase family 1, member E1	4.54
Transporter activity	<i>Rtp3</i>	Receptor transporter protein 3	- 2.05	0.001
	<i>Slc25a30</i>	Solute carrier family 25, member 30	- 2.04	0.002
	<i>Slc38a2</i>	Solute carrier family 38, member 2	- 2.11	0.003
Miscellaneous	<i>Coq10b</i>	Coenzyme Q10 homolog B (<i>S. cerevisiae</i>)	- 2.07	0.004
	<i>Herpud1</i>	Homocysteine-inducible, endoplasmic reticulum stress-inducible, ubiquitin-like domain member 1	- 2.18	0.01
Not determined	<i>n-R5s109</i>	Nuclear encoded rRNA 5S 109	- 2.05	0.002
	<i>n-R5s112</i>	Nuclear encoded rRNA 5S 112	- 2.19	0.002
	<i>n-R5s115</i>	Nuclear encoded rRNA 5S 115	- 2.16	0.002
	<i>n-R5s120</i>	Nuclear encoded rRNA 5S 120	- 2.19	0.002
	<i>n-R5s125</i>	Nuclear encoded rRNA 5S 125	- 2.19	0.002
	<i>n-R5s127</i>	Nuclear encoded rRNA 5S 127	- 2.58	0.002
	<i>n-R5s180</i>	Nuclear encoded rRNA 5S 180	- 2.13	0.01
	<i>n-R5s33</i>	Nuclear encoded rRNA 5S 33	- 2.24	0.003
	<i>n-R5s41</i>	Nuclear encoded rRNA 5S 41	- 2.07	0.01
	<i>n-R5s58</i>	Nuclear encoded rRNA 5S 58	- 2.23	0.003
	<i>n-R5s96</i>	Nuclear encoded rRNA 5S 96	- 2.08	0.004
	<i>Scarna6</i>	Small Cajal body-specific RNA 6	- 2.19	0.001
	<i>Scarna8</i>	Small Cajal body-specific RNA 8	- 2.13	0.02
	<i>Snora36b</i>	Small nucleolar RNA, H/ACA box 36B	- 2.10	0.04
	<i>Snord16a</i>	Small nucleolar RNA, C/D box 16A	- 2.41	0.001
	<i>Snord69</i>	Small nucleolar RNA, C/D box 69	- 2.01	0.01
	<i>Snord92</i>	Small nucleolar RNA, C/D box 92	- 2.37	0.001
	<i>Snord98</i>	Small nucleolar RNA, C/D box 98	- 2.09	0.001

genes are involved in TLR4 activation. In fact, RT-qPCR analysis confirmed the downregulation of *Clec7a* and *Lbp* gene levels in the CCl₄-treated *Panx1*^{-/-} mice. In particular, *Clec7a* is mainly localized in dendritic cells and

macrophages and counteracts the fibrotic response by suppressing TLR4 signaling (Seifert et al. 2015). This could suggest that interference of the NF-κB/Nalp3 signaling axis via *Panx1* deletion reduces inflammatory responses



corresponded to the categories: BDL independent of genetic background or BDL in Panx1^{-/-} genetic background. Results were analyzed by one-way ANOVA followed by post hoc tests using Bonferroni correction. Data were expressed as means \pm SEM (** $p \leq 0.001$). *N.M.* not modulated

and thus the fibrotic response, upon CCl₄ treatment. In contrast, increased transcription of the *S100a9* gene in BDL-subjected Panx1^{-/-} mice was observed. *S100a9* has recently been associated with inflammatory macrophages (Krenkel and Tacke 2017; Simard et al. 2013). In fact, several genes were identified in the BDL Panx1^{-/-} genetic background cluster to be involved in chemotaxis and acute-phase reaction *Cxcl14*, *Hp*, *Plscr1* and *Saa2*, NF- κ B signaling pathway (*S100a6*), and adaptive immune response (*Rnf125*). Nevertheless, RT-qPCR analysis revealed an absence of significant modulation of *S100a9* and *Cxcl14*.

In conclusion, this study shows for the first time an etiology-dependent role for Panx1 signaling in experimental liver fibrosis. Nevertheless, a more in-depth understanding of the mechanisms underlying the Panx1-dependent inflammatory response will require further investigation to assess the therapeutic potential of Panx1 channels as immunomodulators of the fibrotic response.

Acknowledgements This work was supported by the grants of the “Fundação de Auxílio à Pesquisa do Estado de São Paulo” (FAPESP Grants 14/23890-4; 14/23887-3 and SPEC 13/50420-6), the European Research Council (ERC Starting Grant 335476), the Fund for Scientific

Research-Flanders (FWO Grants G009514N and G010214N) and the University Hospital of the Vrije Universiteit Brussel-Belgium (“Willy Gepts Fonds” UZ-VUB). The authors thank Miss Tineke Vanhalewyn, Miss Dinja De Win and Mr Steven Branson for their dedicated technical assistance.

Compliance with ethical standards

Conflict of interest The authors declare that they have no conflict of interest.

Ethical approval All applicable international, national, and/or institutional guidelines for the care and use of animals were followed.

References

- Bao Y, Chen Y, Ledderose C, Li L, Junger WG (2013) Pannexin 1 channels link chemoattractant receptor signaling to local excitation and global inhibition responses at the front and back of polarized neutrophils. *J Biol Chem* 288:22650–22657. <https://doi.org/10.1074/jbc.M113.476283>
- Cai SY, Ouyang X, Chen Y et al (2017) Bile acids initiate cholestatic liver injury by triggering a hepatocyte-specific inflammatory

- response. *JCI Insight* 2:e90780. <https://doi.org/10.1172/jci.insight.90780>
- Canbay A, Taimr P, Torok N, Higuchi H, Friedman S, Gores GJ (2003) Apoptotic body engulfment by a human stellate cell line is profibrogenic. *Lab Invest* 83:655–663
- Chekeni FB, Elliott MR, Sandilos JK et al (2010) Pannexin 1 channels mediate ‘find-me’ signal release and membrane permeability during apoptosis. *Nature* 467:863–867. <https://doi.org/10.1038/nature09413>
- Chen W, Xu WH (2015) β -Actin as a loading control: less than 2 μ g of total protein should be loaded. *Electrophoresis* 36:2046–2049. <https://doi.org/10.1002/elps.201500138>
- Cogliati B, Da Silva TC, Aloia TP et al (2011) Morphological and molecular pathology of CCL4-induced hepatic fibrosis in connexin43-deficient mice. *Microsc Res Tech* 74:421–429. <https://doi.org/10.1002/jemt.20926>
- Cogliati B, Crespo Yanguas S, Da Silva TC et al (2016) Connexin32 deficiency exacerbates carbon tetrachloride-induced hepatocellular injury and liver fibrosis in mice. *Toxicol Mech Methods* 26:362–370. <https://doi.org/10.1080/15376516.2016.1190991>
- Crespo Yanguas S, Willebrords J, Johnstone SR et al (2017) Pannexin1 as mediator of inflammation and cell death. *Biochim Biophys Acta* 1864:51–61. <https://doi.org/10.1016/j.bbamc.2016.10.006>
- Csak T, Ganz M, Pespisa J, Kodys K, Dolganiuc A, Szabo G (2011) Fatty acid and endotoxin activate inflammasomes in mouse hepatocytes that release danger signals to stimulate immune cells. *Hepatology* 54:133–144. <https://doi.org/10.1002/hep.24341>
- Dahl G (2015) ATP release through pannexon channels. *Philos Trans R Soc Lond B Biol Sci* 370:20140191. <https://doi.org/10.1098/rstb.2014.0191>
- Davalos D, Grutzendler J, Yang G et al (2005) ATP mediates rapid microglial response to local brain injury in vivo. *Nat Neurosci* 8:752–758
- Dolmatova E, Spagnol G, Boassa D et al (2012) Cardiomyocyte ATP release through pannexin 1 aids in early fibroblast activation. *Am J Physiol Heart Circ Physiol* 303:H1208–H1218. <https://doi.org/10.1152/ajpheart.00251.2012>
- Dunning S, Ur Rehman A, Tiebosch MH et al (2013) Glutathione and antioxidant enzymes serve complementary roles in protecting activated hepatic stellate cells against hydrogen peroxide-induced cell death. *Biochim Biophys Acta* 1832:2027–2034. <https://doi.org/10.1016/j.bbadis.2013.07.008>
- Dvorianchikova G, Ivanov D, Barakat D et al (2012) Genetic ablation of Pannexin1 protects retinal neurons from ischemic injury. *PLoS One* 7:e31991. <https://doi.org/10.1371/journal.pone.0031991>
- Eaton SL, Roche SL, Llaverro Hurtado M et al (2013) Total protein analysis as a reliable loading control for quantitative fluorescent Western blotting. *PLoS One* 8:e72457. <https://doi.org/10.1371/journal.pone.0072457>
- Gandhi CR (2012) Oxidative stress and hepatic stellate cells: a paradoxical relationship. *Trends Cell Mol Biol* 7:1–10
- Hao H, Cao L, Jiang C et al (2017) Farnesoid X receptor regulation of the NLRP3 inflammasome underlies cholestasis-associated sepsis. *Cell Metab* 25:856–867. <https://doi.org/10.1016/j.cmet.2017.03.007>
- Hara T, Bacon KB, Cho LC et al (1995) Molecular cloning and functional characterization of a novel member of the C-C chemokine family. *J Immunol* 155:5352–5358
- Imamura M, Ogawa T, Sasaguri Y, Chayama K, Ueno H (2005) Suppression of macrophage infiltration inhibits activation of hepatic stellate cells and liver fibrogenesis in rats. *Gastroenterology* 128:138–146. <https://doi.org/10.1053/j.gastro.2004.10.005>
- Jiang S, Zhang Y, Zheng JH et al (2017) Potentiation of hepatic stellate cell activation by extracellular ATP is dependent on P2X₇-mediated NLRP3 inflammasome activation. *Pharmacol Res* 117:82–93. <https://doi.org/10.1016/j.phrs.2016.11.040>
- Karlmarmk KR, Weiskirchen R, Zimmermann HW et al (2009) Hepatic recruitment of the inflammatory Gr1 + monocyte subset upon liver injury promotes hepatic fibrosis. *Hepatology* 50:261–274. <https://doi.org/10.1002/hep.22950>
- Kim HY, Kim SJ, Lee SM (2015) Activation of NLRP3 and AIM2 inflammasomes in Kupffer cells in hepatic ischemia/reperfusion. *FEBS J* 282:259–270. <https://doi.org/10.1111/febs.13123>
- Kowal JM, Haanes KA, Christensen NM, Novak I (2015) Bile acid effects are mediated by ATP release and purinergic signalling in exocrine pancreatic cells. *Cell Commun Signal* 13:28. <https://doi.org/10.1186/s12964-015-0107-9>
- Krenkel O, Tacke F (2017) Liver macrophages in tissue homeostasis and disease. *Nat Rev Immunol* 17:306–321. <https://doi.org/10.1038/nri.2017.11>
- Krick S, Wang J, St-Pierre M, Gonzalez C, Dahl G, Salathe M (2016) Dual oxidase 2 (Duox2) regulates pannexin 1-mediated ATP release in primary human airway epithelial cells via changes in intracellular pH and not H₂O₂ production. *J Biol Chem* 291:6423–6432. <https://doi.org/10.1074/jbc.M115.664854>
- Livak KJ, Schmittgen TD (2001) Analysis of relative gene expression data using real-time quantitative PCR and the 2^{(-Delta Delta C(T))} Method. *Methods* 25:402–408. <https://doi.org/10.1006/meth.2001.1262>
- Maes M, McGill MR, da Silva TC et al (2016) Involvement of connexin43 in acetaminophen-induced liver injury. *Biochim Biophys Acta* 1862:1111–1121. <https://doi.org/10.1016/j.bbads.2016.02.007>
- Maes M, McGill MR, da Silva TC et al (2017) Inhibition of pannexin1 channels alleviates acetaminophen-induced hepatotoxicity. *Arch Toxicol* 91:2245–2261. <https://doi.org/10.1007/s00204-016-1885-6>
- Moles A, Murphy L, Wilson CL et al (2014) A TLR2/S100A9/CXCL-2 signaling for neutrophil recruitment in acute and chronic liver injury in the mouse. *J Hepatol* 60:782–791. <https://doi.org/10.1016/j.jhep.2013.12.005>
- Pradere JP, Kluwe J, De Minicis S et al (2013) Hepatic macrophages but not dendritic cells contribute to liver fibrosis by promoting the survival of activated hepatic stellate cells in mice. *Hepatology* 58:1461–1473. <https://doi.org/10.1002/hep.26429>
- Puche JE, Lee YA, Jiao J et al (2013) A novel murine model to deplete hepatic stellate cells uncovers their role in amplifying liver damage in mice. *Hepatology* 57:339–350. <https://doi.org/10.1002/hep.26053>
- Rivero-Gutiérrez B, Anzola A, Martínez-Augustín O, de Medina FS (2014) Stain-free detection as loading control alternative to Ponceau and housekeeping protein immunodetection in Western blotting. *Anal Biochem* 467:1–3. <https://doi.org/10.1016/j.ab.2014.08.027>
- Saito JM, Bostick MK, Campe CB, XU J, Maher JJ (2003) Infiltrating neutrophils in bile duct-ligated livers do not promote hepatic fibrosis. *Hepatol Res* 25:180–191. [https://doi.org/10.1016/S1386-6346\(02\)00247-4](https://doi.org/10.1016/S1386-6346(02)00247-4)
- Schindelin J, Rueden CT, Hiner MC, Eliceiri KW (2015) The ImageJ ecosystem: an open platform for biomedical image analysis. *Mol Reprod Dev* 82:518–529. <https://doi.org/10.1002/mrd.22489>
- Seifert L, Deutsch M, Alothman S et al (2015) Dectin-1 regulates hepatic fibrosis and hepatocarcinogenesis by suppressing TLR4 signaling pathways. *Cell Rep* 13:1909–1921. <https://doi.org/10.1016/j.celrep.2015.10.058>
- Seki E, Schwabe RF (2015) Hepatic inflammation and fibrosis: functional links and key pathways. *Hepatology* 61:1066–1079. <https://doi.org/10.1002/hep.27332>
- Simard JC, Cesaro A, Chapeton-Montes J et al (2013) S100A8 and S100A9 induce cytokine expression and regulate the NLRP3

- inflammasome via ROS-dependent activation of NF- κ B. *PLoS One* 8:e72138. <https://doi.org/10.1371/journal.pone.0072138>
- Tag CG, Sauer-Lehnen S, Weiskirchen S et al (2015) Bile duct ligation in mice: induction of inflammatory liver injury and fibrosis by obstructive cholestasis. *J Vis Exp* 96:52438. <https://doi.org/10.3791/52438>
- Taylor SC, Posch A (2014) The design of a quantitative western blot experiment. *Biomed Res Int* 2014:361590. <https://doi.org/10.1155/2014/361590>
- Taylor SC, Berkelman T, Yadav G, Hammond M (2013) A defined methodology for reliable quantification of Western blot data. *Mol Biotechnol* 55:217–226. <https://doi.org/10.1007/s12033-013-9672-6>
- Willebrords J, Cogliati B, Pereira IVA et al (2017a) Inhibition of connexin hemichannels alleviates non-alcoholic steatohepatitis in mice. *Sci Rep* 7:8268. <https://doi.org/10.1038/s41598-017-08583-w>
- Willebrords J, Maes M, Pereira IVA et al (2017b) Protective effect of genetic deletion of pannexin1 in experimental mouse models of acute and chronic liver disease. *Biochim Biophys Acta* 1864:819–830. <https://doi.org/10.1016/j.bbadis.2017.12.013>
- Woolbright BL, Jaeschke H (2012) Novel insight into mechanisms of cholestatic liver injury. *World J Gastroenterol* 18:4985–4993. <https://doi.org/10.3748/wjg.v18.i36.4985>
- Wree A, Eguchi A, McGeough MD et al (2014) NLRP3 inflammasome activation results in hepatocyte pyroptosis, liver inflammation, and fibrosis in mice. *Hepatology* 59:898–910. <https://doi.org/10.1002/hep.26592>
- Xiao F, Waldrop SL, Khimji AK, Kilic G (2012) Pannexin1 contributes to pathophysiological ATP release in lipoapoptosis induced by saturated free fatty acids in liver cells. *Am J Physiol Cell Physiol* 303:C1034–C1044. <https://doi.org/10.1152/ajpcell.00175.2012>
- Xiao F, Waldrop SL, Bronk SF, Gores GJ, Davis LS, Kilic G (2015) Lipoapoptosis induced by saturated free fatty acids stimulates monocyte migration: a novel role for Pannexin1 in liver cells. *Purinergic Signal* 11:347–359. <https://doi.org/10.1007/s11302-015-9456-5>
- Xie G, Wang X, Wang L et al (2012) Role of differentiation of liver sinusoidal endothelial cells in progression and regression of hepatic fibrosis in rats. *Gastroenterology* 142:918–927.e6. <https://doi.org/10.1053/j.gastro.2011.12.017>
- Yan HH, Jiang J, Pang Y et al (2015) CCL9 induced by TGF- β signaling in myeloid cells enhances tumor cell survival in the premetastatic organ. *Cancer Res* 75:5283–5298. <https://doi.org/10.1158/0008-5472.CAN-15-2282-T>